AMBIENT TEMPERATURE CREEP BEHAVIOR OF SPARK PLASMA Ti-6Al-4V/TiN COMPOSITES

by

MOKGOBA GLODEAN KGANAKGA

DISSERTATION

Submitted in fulfilment of the requirements for

MASTERS DEGREE

in

ENGINEERING METALLURGY

in the

FACULTY OF ENGINEERING AND THE BUILT ENVIRONMENT UNIVERSITY OF JOHANNESBURG

SUPERVISOR: PROF. PETER APATA OLUBAMBI

CO-SUPERVISOR: DR. OLAWALE OLAREWAJU AJIBOLA

JUNE 2019

DECLARATION

I Mokgoba Glodean Kganakga (201043404) hereby declare that the dissertation, which I herewith submit for the qualification of

MASTERS IN ENGINEERING METALLURGY

to University of Johannesburg, in the Faculty of Engineering and Built Environment, Department of Engineering Metallurgy is my own work and has not been submitted before for any degree or examination in any other university.

Signature : ……..

Date: …24..……/…June……../…2019…….

DEDICATION

I dedicate this dissertation to my parents, Annah Kganakga and Zacheus Kganakga; my sisters, Mokgadi Kganakga and Selaelo Kganakga and my nephew Bohlale Kganakga who have always loved and supported me unconditionally and whose good examples have taught me to work hard for the things I aspire to achieve. I dedicate this work to my late mentor Dr S.W Bhero who has always believed in me and taught me that everything is possible if you keep your eyes focused on the ball. I would also like to dedicate this dissertation to supervisor Professor Peter Olubambi for his constant support, love, and words of encouragement throughout my postgraduate studies.

ACKNOWLEDGEMENTS

This project was a success because of the selfless individuals who took their time to assist and guide me with my project through to completion. I am very privileged to have worked with the following individuals:

Gratitude goes to my supervisor Prof. P.A. Olubambi whose words of inspiration and guidance has sharpened me to the person I have become today. I appreciate his unshaken support, love and words of encouragement. Above all, I am thankful for my co-supervisors Dr O.O. Ajibola and Dr B.A. Obadele for their constant assistance and guidance for my work. I thank them for not losing hope in me when the journey seemed tough.

Special thanks go to all CNT postgraduate students under supervision of Prof P.A Olubambi; Dr W. Turkart and his postgraduate students from UNS in Argentina; Extraction metallurgy laboratory from University of Johannesburg and Metallurgical Engineering and Material Science at Tshwane university of Technology for assisting me and ensuring equipments availability for my project.

Special gratitude goes to my parents; Annah Kganakga and Zacheus Kganakga, my sisters, Mokgadi kganakga and Selaelo kganakga and my nephew Bohlale Kganakga. I appreciate them for their robust support and tethered love that kept me going against all odds.I am thankful for my colleagues (Nicolene Mekgwe, Mosima Maja, Mukhethwa Netshia and Noxolo Amalgues) for their unwavering assistance on my experimental works. I hereby acknowledge the individuals whose published intellectual articles are referred and all host of others whose unpublished technical advices have contributed a great deal to the success of this work.

I would like to acknowledge National Research Foundation (NRF) of South Africa for granting me scholarship to pursue my postgraduate studies. Above all I would like to thank the Almighty God for sustaining and giving me strength to complete this work.

ABSTRACT

Ti-6Al-4V alloys are well known for their high strength to weight ratio, corrosion resistance, fatigue and high temperature properties. In this Study, the effect of TiN addition on the mechanical properties of spark plasma sintered Ti-6Al-4V alloys was investigated. Ti-6Al-4V alloy powders with different proportions of TiN (2, 4 and 6%) were produced using Spark Plasma Sintering (SPS). Further, the spark plasma sintered samples were analysed using scanning electron microscopy, X-ray diffraction and optical microscope. The spark plasma sintered samples were then investigated for mechanical behaviours such as creep, erosion-wear and wear response. Creep, modulus of elasticity and hardness properties were investigated using the nanoindentation technique equipped with Berkovich indenter. On the other hand, high velocity solid particle erosion test was used to examine the erosion-wear behavior of Ti-6Al-4V alloy with and without TiN additions. The aim and objectives of the research was to understand how different proportions of TiN addition affect the creep and erosion wear response of Ti-6Al-4V-TiN composite, investigate the mechanisms of creep on the using nanoindentation test, and evaluate the mechanism of wear occurring on the nano-composites and to characterize and analyse surface morphologies and fracture mode of SPS Ti6Al-4V-TiN composites. The results revealed that the use of SPS technique and TiN nanoparticles has led to transformation from alpha/beta lamellar to bimodal microstructure. It was also noticed that the presence of TiN improves the mechanical properties of Ti-6Al-4V to some extend and lead to deterioration as the volume fraction of TiN goes to 4% volume fraction. Nanoindentation results revealed that elastic modulus and hardness increased drastically with increase in TiN addition. Increasing the applied load reduced the hardness and elastic modulus. Ti-6Al-4V+ 6% TiN presented improved mechanical properties such as erosion wear, abrasive wear and creep resistance.

TABLE OF CONTENTS

LIST OF FIGURES

LIST OF TABLES

LIST OF ACRONYMS

AC	Contact Area
AM	Additive Manufacturing
BCC	Body Centered Cubic
CIT	Creep Indentation
CNT	Center of Nano-engineering and Tribocorossion
CPT	Commercially Pure Titanium
D	Diameter
EDS	Energy Dispersive Spectroscopy
EI	Indentation Elastic-modulus
HCP	Hexagonal Closed Packed Structure
HIP	Hot Isostatic Pressing
HIT	Indentation Hardness
HVSPE	High Velocity Solid Particle Erosion
MMC	Metal Matrix Composites
Min	Minutes

OM	Optical Microscope
SEM	Scanning Electron Microscope
SPS	Spark Plasma Sintering lessen
3DP	Three Dimensional Printing
Ti-6Al-4V	Titanium-6w%Aluminium-4w%Vanadium
TiCl4	Titanium Tetrachloride
TRB	Tribometer

CHAPTER ONE: INTRODUCTION

The increasing use of engineering materials in severe environments requires a material that exhibits good mechanical properties (Bahaideen et al., 2009). Titanium and its alloys are extensively used in many structural applications due to their unique combination of mechanical and physical properties which have made them desirable for aerospace, industrial, chemical power generation, oil and gas, marine and architecture (Zhang et al., 2014). Ti-6Al-4V alloy represents an important class of titanium alloys comprising of the alpha (α) and beta (β) phases.

Regardless of their superior properties just like any other alloy they have shortcomings. Titanium alloys are reported to show significant room temperature creep even at stress below the yield strength. It is believed that the relatively low work-hardening rates in titanium and its alloys lead to explicit low temperature creep (Huang et al., 2017). Moreover, lack of slip systems in titanium alloys lead to poor creep resistance at both lower and high temperatures (Abdallah et al., 2013).

On the other hand, since Ti-6Al-4V alloys have found the most exclusive application in the manufacture of rotor blades of jet engines, it is quite evident that such components are faced with serious challenges of erosion due to combustion system and environmental factors especially at high temperatures (Sharma et al., 2017). According to Naveed et al. (2015) usual atmospheric situations such as volcano ashes, sand storms, and ice particles induce erosion damage on aero-engines. Dust ingested by turbines induces erosion damage of its components, especially at the first-stage compressor blades, resulting in low performance (Naveed et al., 2015).In spite of all the efforts made to mitigate the failure of structural materials in the industry, creep and fatigue still contribute to failure of most materials. Regardless of what has been mentioned in the latter, the creep failures in the aerospace industry are now extremely rare due to the fact that creep testing equipment have been designed such that they imitate real life loading for aircraft structures (Tao et al., 2014).

In an attempt to solve some of the problems associated with titanium and its alloys, several approaches were adopted. Metal-matrix composites were used to salvage the mechanical properties of such alloys. In MMC, hard particle materials are reinforced either in the form of fibre, whiskers or second phase particles in the matrix of alloys such as aluminium, magnesium and titanium (Mouritz, 2012). On that account, TiN nano-ceramic was considered as the

potential candidate due to its outstanding mechanical properties (Falodun et al., 2018). TiN and its derivative materials have triggered great interest due to their remarkable properties such as thermal stability, high hardness, high fracture toughness and oxidative resistance (Guo et al., 2015). In this study TiN nanoparticles have been reinforced in Ti-6Al-4V matrix to improve the mechanical properties such as wear and creep.

The process of manufacturing nanoparticle ceramic dispersion reinforcing titanium alloys using the technique of melting and casting is related to the control of grain sizes during solidification, and non-uniform dispersion of the nanoparticle ceramic. This could be because of differences in density, melting point, and thermal conductivity among the nanoparticle and titanium matrix. However, researchers have reported that powder metallurgy (PM) could be another technique for fabrication of dispersion strengthened titanium alloys (Falodun et al., 2018). Conventional melting has disadvantages of producing excessive contamination of the alloy, poor control of the microstructural evolution and lack of surface finish after casting. Unlike melting, hot isostatic pressing and conventional sintering methods are capable of producing near net shape products. However, they usually require high sintering temperature and long sintering time resulting in grain growth of the final structure (Bayode, 2016).

Spark plasma sintering technique was used in several studies to produce Ti-6Al-4V+TiN nanoceramics. SPS has gained a leverage over other alloying techniques because of its high sintering speed. Spark plasma sintering (SPS) emerged as a relatively novel powder metallurgical technique, which requires less sintering time, the ability to produce near net shape products and fully dense microstructure with no grain grown (Bayode, 2016). In SPS technology, the raw powder is loaded into the graphite die, vertical pressure and a pulsed electric current voltage is passed through the die. The sintering temperature is monitored using thermocouple for temperatures below 1000˚C and a pyrometer for temperatures above 1000˚C. The SPS enables one to have a proper control of the sintering parameters and mechanical properties (Bayode, 2016). Thus in this study, spark plasma sintering will be used to consolidate Ti-6Al-4V+TiN nano-composites.

Finally, before a material is deemed fit for use, it has to go through the mechanical testing process equivalent to the service environment to test if it can withstand the service conditions. With that said, the nanoindentation technique has emerged as a non-destructive method for testing the mechanical response of a material to an applied load. It enables investigations of

material under dynamic conditions which offer direct measurements of hardness, elastic modulus, creep and fatigue test of a material (Maja et al., 2018). This is done through the continuous recording of applied force and resulting depth penetration of the indenter throughout the loading and unloading cycle. It can continuously measure force and displacement as indentations are made without disrupting the microstructure (Lucca et al., 2010). Therefore, nanoindentation technique will be used to examine the mechanical properties in this study.

1.1 Research Problem Statement

One of the shortcomings of Ti-6Al-4V alloys is their proneness to creep at temperatures above 400^{o}C, attributed to loss of strength and toughness (Dai et al., 2016). Studies also revealed that due to their low-work hardening properties titanium alloys present room temperature creep even at stress below the yield strength. Moreover, Ti-6Al-4V alloys have found the most exclusive application in the manufacture of rotor blades of jet engines, it is quite evident that such components are faced with serious challenges of erosion wear attributed to combustion system and environmental factors especially at high temperatures (Sharma et al., 2017). Dust ingested by turbines induces an erosion damage of its components, especially at the first-stage compressor blades, resulting in low performance (Naveed et al., 2015).

A novel Ti-6Al-4V+TiN composite was developed with the expectation of improving mechanical properties and widening the high temperature application range of Ti-6Al-4V alloys. However, the properties of the alloy are not yet understood, which propelled this research study. Previous studies examined the mechanical properties such as modulus of elasticity and hardness (Maja et al., 2018). Little is understood on the nano-indentation-creep behaviour and erosion-wear of nano-crystalline Ti-6Al-4V+TiN composites at lower temperature. Furthermore, another limitation is in the use of nanoindentation testing. Nanoindentation test is a very sensitive technique in the sense that it is sensitive to noise, vibration and people's movement, which cause the pop-in and pop-out effect when contracting the load displacement curves. It also requires a sample to be flat and smooth (Mphahlele, 2018).

1.2 Research Questions

- How does the presence of TiN nano-ceramic affect the nanoindentation creep strength of spark plasma sintered Ti-6Al-4V alloy?
- What could be the overall effect of the nanoindentation on the modulus of elasticity and hardness of Ti-6Al-4V+TiN?
- What is the combined effect of spark plasma sintering and nano strengthening on the overall mechanical response of Ti-6Al-4V alloy?

1.3 Aims and Objectives

The aim of this research is to investigate the nanoindentation creep resistance and erosion-wear behaviour of spark plasma sintered Ti-6Al-4V+TiN composites. The specific objectives of this research include:

- Studying the effect of spark plasma sintering on the microstructural evolution of Ti6Al4V+TiN samples.
- Investigating how different proportions of TiN addition affect the creep and erosionwear response of Ti-6Al-4V+TiN composite.
- To understand the stages of creep on using nano indentation test.
- To examine the mechanism of wear occurring on Ti-6Al-4V+TiN composites.
- Analysing surface morphologies of Ti6Al4V+TiN composites after erosion wear.

1.4 Hypothesis

Hypothetically, by the virtue of their outstanding properties, the presence of TiN nanoparticles will improve the creep and wear properties of SPS Ti-6Al-4V alloy. Further, since SPS is known to produce fully dense microstructure with no grain growth due to it's less sintering time (Bayode, 2016), the mechanical properties such as hardness and density are expected to increase.

1.5 Justification of Research

Ti-6Al-4V alloy is the workhorse of the titanium industry and it is extensively used for a wide range of applications (Donachie Jr, 2000). Therefore, it is imperative to understand and improve on the properties of Ti-6Al-4V alloy and how the alloy is comparable to other aerospace application alloys. Moreover, we have come into the fourth industrial revolution were emerging technologies are prioritising the utilization of energy efficient and cost saving materials (Marwala and Hurwitz, 2017). Therefore, Ti-6Al-4V is amongst the light weight cost saving material during service.

A TiN reinforced Ti-6Al-4V composite was newly developed with the view of enhancing the overall thermo-mechanical properties required in the performance of Ti-6Al-4V+TiN in the aero-engines (Falodun et al., 2018). There were only few studies obtained on the mechanical properties of spark plasma sintered Ti-6Al-4V+TiN (Maja et al., 2018). So this study aims to understand the mechanical properties of the composites using nanoindentation and high velocity particle erosion techniques. Studies have shown that creep plays a paramount role

when selecting properties of a material in aerospace industry. In addition, rotational parts such turbines are prone to erosion-wear (Sharma et al., 2017). Therefore, it is imperative to know the creep and wear properties of the composite and how they compare with other creep and wear resistant alloys. Hence, the need arises to reinforce Ti-6Al-4V with some other ceramic materials of importance such as TiN. Moreover, conducting this research will broaden the knowledge area and application range in Ti-6Al-4V alloys.

1.6 Expected Contribution to Knowledge

The demand for materials that can exhibit exceptional mechanical properties over a range of temperatures has become crucial for the aerospace industry. The incorporation of TiN into Ti6Al-4V will improve the mechanical properties and widen the use of Ti6Al-4V for both lower and high temperatures. Producing of Ti-6Al-4V+TiN composite through the use of spark plasma sintering is expected to increase the mechanical properties such as strength, densification, and reduce porosity and permeability of the composite. SPS will also salvage the problem of compositional alloy control, grain growth and poor surface finish. Moreover, SPS will reduce the production time without compromising the quality of the final product.

1.7 Scope of Work

This work involved the use of novel alloy production and mechanical testing techniques such as SPS, high velocity solid erosion and nanoindentation test, with the objective of improving the mechanical properties of the newly developed Ti-6Al-4V+TiN composites. Spark plasma sintering technique was used to produce different compositions of Ti-6Al-4V+TiN composites. The sintered samples were then characterised using SEM (scanning electron microscope), XRD (X-ray- Diffractometer) and OM (optical microscope), for surface morphologies and phase identification. Furthermore, the sintered samples were tested for erosion-wear, hardness, creep resistance and modulus using nanoindentation and high velocity solid erosion test techniques, respectively. Lastly, the surface morphologies of the samples were analysed after conducting the mechanical tests.

1.8 Structure of the Dissertation

Introduction to the research, problem statement, research problem, research questions, aim and objectives, hypothesis, the justification of the research, expected outcomes and scope of work are discussed in **Chapter one**. **Chapter Two** entails the literature review on MMCs, Titanium alloys, creep and erosion-wear, spark plasma sintering technique, high velocity solid erosion

test and nano-indentation technique. In **Chapter Three** the experimental works of this research project are discussed. **Chapter Four** gives detailed results obtained from the experiments and discussions based on the fundamental scientific principles. In **Chapter Five**, the conclusions and recommendations are presented based on the observations and the results obtained in the study.

CHAPTER 2: LITERATURE REVIEW

2.1 Introduction

This chapter entails the overview on metal matrix composites, titanium alloys and their applications, and powder metallurgy processes. It also explains the mechanical properties of interest such as creep, erosion-wear and wear. Finally the high temperature high velocity test and nanoindentation techniques are discussed as the methods used for testing in this research study.

2.2 Metal Matrix Composites

Composites are group of materials produced when two or more materials or phases are combined to give a distinct property from original materials. They are classified into metal matrix composites, ceramic matrix composites, polymer matrix composites, carbon matrix composites and hybrid matrix composites (Saxena et al., 2017, Yu et al., 2019). Metal matrix composites refers to a class of composites in which a hard ceramic reinforcement is dispersed in the matrix of the ductile metal matrix. In instances where a ceramic is dispersed as nanoparticles the composite is termed metal matrix nano-composites (MMNs). Metal matrix nanocomposites yield a combination of metallic properties like ductility and toughness and nanoceramic properties such as hardness, high strength and modulus (Gupta et al., 2018). Metal matrix nano-composites have gained potential application in the aerospace ,automotive and defence industries, due to their superior properties such as high strength to weight ratio, density, fatigue and great wear resistance (Mphahlele, 2018, Almotairy et al., 2019).The overall mechanical properties of MMNCs is determined by factors such as homogeneous distribution, properties of the reinforcement material, the interfacial reaction between the reinforcement and the matrix material and the volume fraction of the reinforced material (Saxena et al., 2017).

2.3 Titanium alloys and their applications

Titanium alloys have been extensively used in most engineering applications at low and high temperatures. Titanium is a low density, high melting point metallic element widely used for structural and nano-structural purposes for its high toughness, exceptional corrosion resistant, high strength to density ratio and balanced elevated temperature properties. Titanium is a transitional metal, distinct from other light metals such as aluminium and magnesium. It has a high solubility for several other elements and high reactivity with interstitial elements such as oxygen, nitrogen, hydrogen, and carbon (Moorhouse, 2013). Titanium and its alloys exhibit a unique combination of mechanical and physical properties which have made them desirable for

aerospace, industrial, chemical power generation, oil and gas, marine and architectural (Dai et al., 2016).

2.3.1 Titanium alloy grades

Titanium alloys are classified into three major groups. The categories are the α-alloys, β- alloys and the α+β alloys. Their properties depend on chemical composition and thermo-mechanical processes involved, which as a result affect the final microstructure (Veiga et al., 2012). At lower temperatures, titanium and its alloys crystalize in an ideally modified hexagonal closed packed structure, and it is said to be alpha titanium. At high temperatures, it crystalizes as body centered cubic, beta titanium, as shown in Figure 2.1

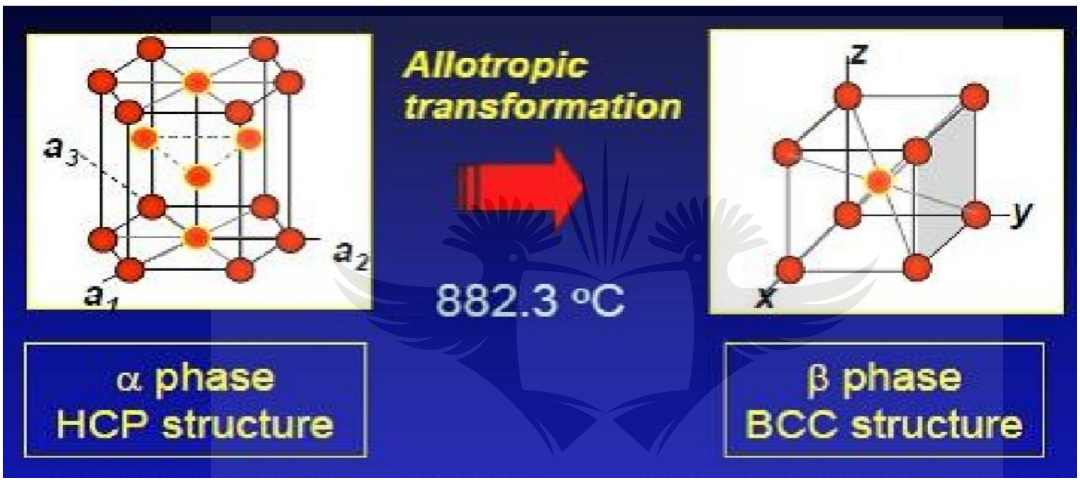

Figure 2. 1. Crystal structure of commercially pure Ti at room and high temperatures (Wooding and Laubscher, 2014).

However, two crystal structures (α and β) can exist concurrently at lower and high temperatures by addition of alloying elements. The alpha phase stabilizers are carbon, nitrogen, oxygen, which form the interstitial solid solutions in titanium. Addition of such elements stabilizes the existence of the alpha phase at high temperature by raising the alpha-beta transformation temperature, in this case the alpha phase will be able to exist over a wide range of temperatures. The beta stabilising elements such as vanadium, copper, chromium and molybdenum lower α +β transformation temperatures (Watkins, 2015). Figure 2.2 shows how the additions of alloying elements affect the movement of the α +β transus temperature. The three categories of the alloys are discussed below.

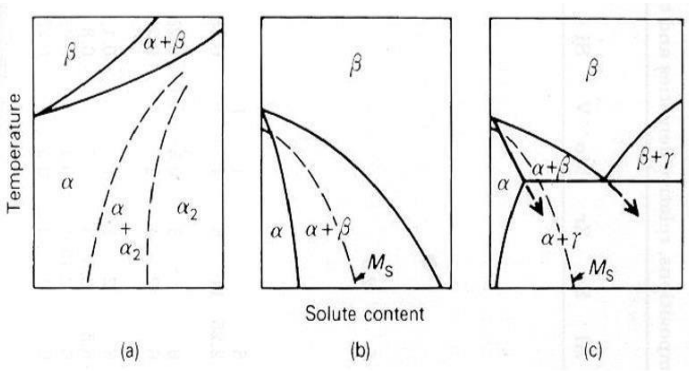

Figure 2. 2. Phase diagrams of Ti with added alpha and beta stabilisers (Obadele, 2014).

2.3.1.1 Alpha (α) Titanium Alloys

Generally, α-alloys are single solid solutions of the alpha phase. Alpha titanium alloys possess good high temperature properties, weldability, toughness and better creep properties. The mechanical properties of alpha alloys cannot be improved by microstructural modification but can be strengthened through solid solution strengthening. In the solid solution strengthening the solute atoms act as a dislocation barrier thereby increasing the internal stress of the alloy (Wang et al., 2016). Alpha titanium alloys are mostly used for producing cryogenic vessels (Veiga et al., 2012).

The prime elements such as aluminium and oxygen, are responsible for stabilizing alpha phase at all temperature range (Polmear et al., 2017). Aluminium and oxygen raise the $\alpha \rightleftharpoons \beta$ transformation temperature making the alpha phase to exist over a range of temperatures, as shown in Figure 2.2. The alpha phase region grows bigger at the expense of the beta phase even at high temperatures. When these elements dissolve in titanium, they tend to repel and get diluted in titanium and Ti-Ti bond is created; thereby maintaining the HCP microstructural characteristics. Examples of alpha titanium alloys are: Ti-5Al-2.5Sn, Ti-8Al-1Mo-1V and Ti5Al-4Sn-2Zr-1Mo-0.25Si-1Ni (Obadele, 2014).

2.3.1.2 Beta (β) Titanium Alloys

The β-alloys (beta titanium alloys) contain a large amount of beta stabilizers such as Mo, V and Cr. Annealing of β titanium alloys produces a significant increase in strength and reduced ductility and toughness. Upon quenching of beta titanium alloys in the beta phase region, a single beta phase with bcc structure is retained. Consequently, this gives the beta alloys the excellent combination of properties which includes strength, toughness, and plastic properties. The strength of β titanium alloys is associated with the precipitation of the primary/secondary alpha phase during thermo-mechanical processing. The α phase acts as a barrier to inhibit the dislocation movement, causing the precipitation of the microstructure. The beta titanium alloys

are limited to low strength applications due to the lower ductility and toughness. Beta titanium alloys are mostly used as fasteners and springs and their examples are Ti-3Al-8V-6Cr-4Mo4Zr, Ti-15V-3Cr-3Sn-3Al and Ti-3.5Al-5Mo-6V3Cr-3Sn-0.5Fe (Obadele, 2014).

2.3.1.3 Alpha (α) + Beta titanium (β) alloys

The alpha/beta alloys are a group of alloys which contain both α + β phases below the β temperatures. Four to six percentage of alpha stabilizers are added to give strength to the alloy. Conversely, β stabilizers are added to allow β phase to be retained at lower temperatures. The alpha/beta titanium alloys exhibit properties such as good heat treatment, good forming properties, medium to high strength and good creep strength, which, make them desirable for most engineering applications (Muhammad et al., 2018). This group of alloys are widely used in the aerospace industry and machine components (Wooding and Laubscher, 2014). The typical example of α+β alloys is Ti-6Al-4V.

Ti-6Al-4V alloy also known as the work horse of the titanium industry is α+β titanium alloy which contains 6%w Al and 4%w of Vanadium. Ti-6Al-4V alloy was designed for a good balance of characteristics, including: strength, ductility, fracture toughness, high temperature strength, creep characteristics, weldability, workability, and thermal process ability (Ghiban et al., 2018). Furthermore, there are many actual applications of this alloy in aircraft where high reliability is required, further, the availability of abundant data promotes its application. In airframes, it is used for general structural material, bolts, seat rails and the like. In engines, due to the relatively low allowable temperature of about 300˚C, the alloy is used for fan blades, fan case and in the intake section where temperatures are relatively low (Takahashi, 2003).

2.3.2 General applications of Ti-6Al-4V alloy

Titanium alloys, have been used in biomedical, marine, automotive and aerospace industries due to their extensive properties which are corrosion resistance, high elastic modulus, wear resistance high strength and most importantly their biocompatibility characteristics (Guo et al., 2015). In biomedical, Ti-6Al-4V alloys are used for replacing failed hard tissues, as in artificial hip joints, artificial knee joints, bone plates, artificial hearts, and pace makers. The use of Ti6Al-4V alloys in dental implants involves osseo-integrated and orthodontic anchorage (Elias et al., 2013) . Figure 2.3 shows Ti-6Al-4V alloy applications in a hip replacement.

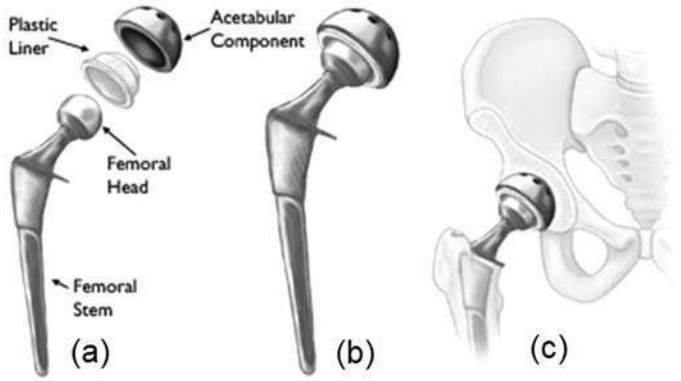

Figure 2. 3. (a) Components of a total hip replacement; (b) The components merged into an implant; (c) The implant as it fits into the hip (Aherwar et al., 2016).

Ti-6Al-4V alloys are used for designing pressure vessels and heat exchangers for marine applications (Yamada, 1996).Ti-6Al-4V alloy are able to form oxide scales at room and high temperature which enables them to resist crevice and pitting corrosion. The alloy only degrades due to corrosion (Gurrappa, 2005). Ti-6Al-4V alloys are dominant in automotive industries for manufacturing the engine and the exhaust valves of two wheel and four wheel vehicles, as in Figure 2.4. Ti-6Al-4V alloys reduce the weight of the components which leads to a subsequent increase in the fuel efficiency and power out-put.

Figure 2. 4. Vehicles components made from Ti-6Al-4V alloys (Takahashi, 2003).

Ti-6Al-4V alloys find their usage in a variety of components in the aerospace, and these include, compressors', turbine blades, bolts, screws and airframes (Kgoete et al., 2018). As far as temperature is concerned, Ti-6Al-4V alloys are used at temperatures lower than 400^{o}C owing to their low oxidation, low creep and fatigue resistance at temperatures above 400^{o}C, as shown in Figure 2.5, showing areas where Ti-6Al-4V is applied i.e Fan blades and low-pressure compressor blades (Azarniya et al., 2019).

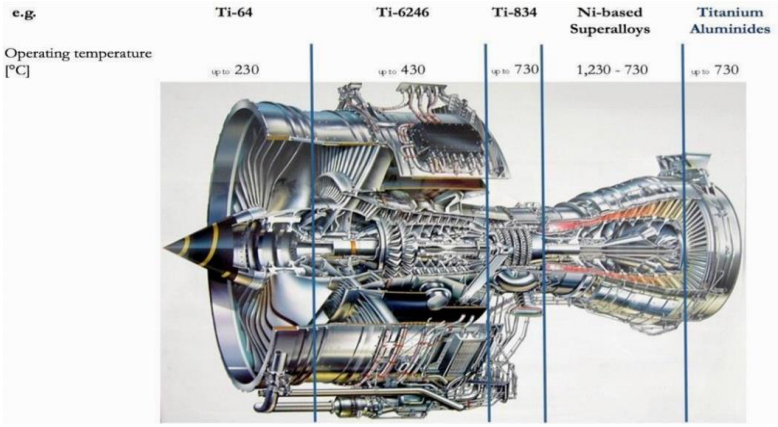

Figure 2. 5. Aero-engine part showing areas where Ti-6Al-4V alloys are used (Azarniya et al., 2019).

2.4 Titanium Nitride Nano-ceramics

Developing of highly incompressible materials with novel mechanical properties has triggered great interest in the high temperature applications. Ceramic materials are used to strengthen and improve the mechanical properties of high temperature structures, as in Figure 2.6. Ceramic materials are characterized by high thermal stability, high hardness, high fracture toughness, and oxidative resistance. Most of all, ceramic materials provide high hardness to the metal matrix composites. Examples of ceramic materials are TiC, WC, Mo, TaC and CoNi . Table 2.1 shows the ceramic materials and the respective compositions (Zhou et al., 2009).

Table 2. 1. Chemical compositions of ceramic materials (Zhou et al., 2009).

Material	C	N	S	O	W	Ti	Ni	Mo	Nb
TiC	18.800	-	0.0270	0.001720	-	Bal.	-	-	-
TiN	0.0890	24.9	0.0012	0.000135	-	Bal.	-	-	-
Ni	0.1780	-	0.0033	0.001060	-	-	Bal.	-	-
Mo	0.0094	-	0.0072	0.001215	-	-	-	Bal.	-
WC	6.11	-	0.0026	0.001020	Bal.	-	-	-	-

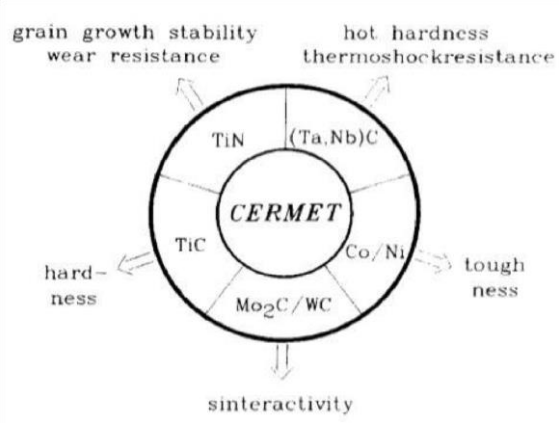

Figure 2. 6. Cermet materials and properties (Ettymayer et al., 1995)

TiN has triggered an interest of many researchers owing to its high thermal stability, high hardness, high fracture toughness and oxidative resistance (Yu et al., 2015). TiN nano-ceramic are thermo chemically stable and inert when subjected to corrosive environments. Generally, they are used as coating materials in cutting and drilling tools owing to their extremely high hardness and wear resistance. They are also used as superconducting materials due their low electrical resistivity (Zhou et al., 2019). Russias et al. (2005) Observed that the presence of TiN addition in the alloy matrix inhibits the rate of grain growth. Consequently, the grain size gets reduced and the hardness of the alloy increases.

Nonetheless, the mechanical properties of Ti(C,N) were investigated as a function of nitrogen content. It was observed by Cardinal et al. (2009) that as the Nitrogen content goes high the mechanical properties such as electrical resistivity and heat conduction increases, whereas, the hardness decreases. In such context, Shi et al. (2017) reported the improvement in thermodynamic stability and change in slip systems with increasing Nitrogen concentration. Russias et al. (2005) Advocate that TiN addition below 6w% improves the mechanical properties and leads to deterioration in mechanical properties as the TiN addition goes above 6w%. Tabulated chemical composition of TiN is presented in Table 2.2 .

Table 2. 2. Chemical composition of TiN ceramic (Zhou et al., 2009).

Element	C	N	S	O	W	Ti	Ni	Mo	Nb
w%	0.0890	24.9	0.0012	0.000135	-	Bal.	-	-	-

Mahesh et al. (2017) & Zgalat-Lozynskyy et al. (2012) conducted studies on the effect of TiN particulates reinforcement on the mechanical properties of metal matrix. TiN particulates and the metal matrix powders were sintered in a tube furnace at varying temperatures. It was

observed that there was an increase in densification, hardness, and surface roughness, with an increase in TiN content. In addition, a study on TiN and TiCN coatings on Ti and Ti-6Al-4V alloy on the mechanical properties was performed. The nano-indentation test was used to determine the Young's modulus and hardness of the alloy after coating. Fracture behavior of the coatings was studied using spherical diamond indenter with diameter of 5 μm, maximum loads of 160 mN, 260 mN and 360 mN. Fracture was evaluated at the loading/unloading rate of 200 μN/s .The TEM observations showed the presence of inclined cracks, radial cracks, inter-column and lateral cracks (Sun et al., 2014). Furthermore, Farokhzadeh and Edrisy (2015) investigated the fatigue response of Ti-6Al-4V alloy using plasma nitriding technique. The fatigue resistance of Ti-6Al-4V alloys at 600^{o}C increased due to the formation of hard TiN precipitates on the surface. The fatigue response further deteriorates as the temperature goes to 900^{o}C due to the formation of hard alpha case which act as crack initiation sites.

2.5 Powder Metallurgy Fabrication Methods

Powder metallurgy is a process of mixing and blending powders to produce an alloy. After the alloy is produced, techniques which involves, hot isostatic pressing, additive manufacturing, hybrid spark plasma sintering and spark plasma sintering are used to produce a fully dense alloy. Unlike other conventional methods powder metallurgy process is capable of producing near net shape products, intricate shapes and less material wastage (Donachie Jr, 2000).

2.5.1. Hot isostatic pressing

Hot isostatic pressing (HIP) is a powder pressing technique which uses high pressure to consolidate green compacts. Procedurally, the metal powder is put inside a die and high isostatic pressure is applied. Then high temperature is applied to create bonding between the metallic powders resulting in a fully dense product. The technique is provided with heating and cooling systems which enable the compacted material to heat and cool fast (Tam et al., 2009). Chmiela et al. (2016) Reported a reduction in porosity and betterment in mechanical properties when HIP was used. High pressure and higher temperatures lead to faster diffusion rate and porosity collapse (Tammas-Williams et al., 2016). Theoretical diagram of the technique is shown in Figure 2.7.

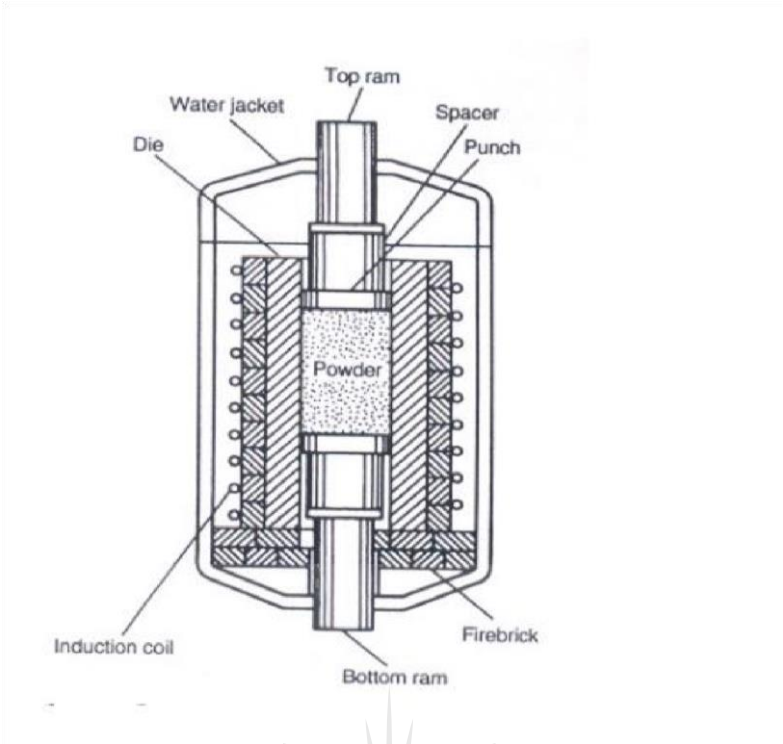

Figure 2. 7. Generic diagram of hot isostatic pressing (Tammas-Williams et al., 2016).

Nonetheless, the use of this technique reduced as it brought about negative impacts on the mechanical properties of the alloy. Long sintering times and high temperatures led to grain growth in the final microstructures resulting in deterioration in mechanical properties. In addition, HIP lacks the modelling tools for predicting geometrical changes that occur during the consolidation process (Essa et al., 2016).

2.5.2 Additive manufacturing

Additive manufacturing (AM) was first introduced in the 1980s when lots of technologies emerged. AM is powder metallurgy manufacturing processes which involves a layer by layer manufacturing of 3D printing objects. This technology uses well formatted data to construct 3D layers, as shown in Figure 2.8 (Jiang et al., 2018). It is used to manufacture parts in aerospace, automotive, defense, dental implants and otherwise. It is subdivided into 5 major groups, which are, laser melting fusion, laser metal deposition, selective laser sintering, wire arc additive manufacturing and thermal spraying surface finish. Additive manufacturing is found for group of materials such as, ceramics, metals and polymers. It has generated US$ 5.1 billion for USA revenues and it is expected to generate US$21 billion of revenues by 2020, which is an indication that is it has triggered a positive impact and it is also growing at an exponential rate (Jiang et al., 2018).

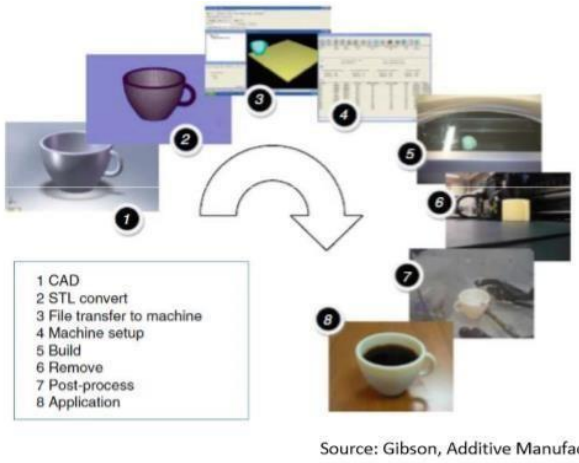

Figure 2. 8. Generic process of AM technology (Jiang et al., 2018).

Additive manufacturing is capable of producing objects of highest intricate shapes and geometries at a reduced production time. It is cost effective and energy saving. Furthermore is has the ability to redesign the same product but with improved mechanical properties. It is also well designed to fit for the fourth industrial revolution which makes it applicable for many more decades to come. However, the adoption of AM technology by industries is limited to high purchasing cost, high maintenance, and lack of well-trained personnel's (Wu et al., 2017).

2.5.3. Spark plasma sintering

Spark plasma sintering (SPS) also known as pulsed current sintering, is one of the most used powder metallurgy techniques. It has been widely used by numerous industries since its inception in 1970s (Bayode, 2016). In SPS process, the blended powder is consolidated inside a graphite die. Due to its good thermal and electrical properties it enables heat to be transferred at lower voltages. The consolidation of the powder involves passing of pulsed electric current on the graphite die at high heating rate(100^{o}C/min) and high pressure (Han et al., 2016), as shown in Figure 2.9.

In such context, SPS is capable of producing fully dense microstructures with less or no grain growth at all. Low grain growth is attributed to low sintering times and temperatures. However, the expensive pulsed electric current and lack of production of asymmetric shapes limit its adoption (Saheb et al., 2012).

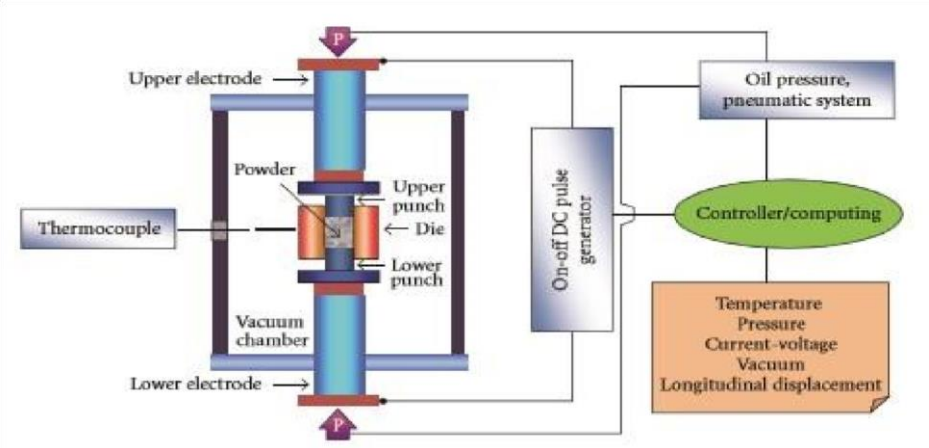

Figure 2. 9. Spark plasma sintering process (Saheb et al., 2012).

2.6. Mechanical properties

Metallic materials are used in design of most components and structures, due to their mechanical properties such as the ability to withstand high service loads (Carrion et al., 2017). The increasing use of engineering materials in severe environments requires a material that exhibits good mechanical properties (Bahaideen et al., 2009). Most structural materials are subjected to creep under normal operating conditions that can result in a catastrophic failure. Consequently, the metal characteristics, particularly the aspect of metal creep, attracts consistent attention of scientists, engineers and designers (Carrion et al., 2017). Thus, it is imperative to understand the mechanism of creep, because, although precise values are not available, it is expected that at least half of all mechanical failures are related to fatigue and creep. In the USA, approximately 4% of the gross national product are related to creep and fatigue failures .In spite of all the efforts made to mitigate the failure of structural materials in the industry, creep and fatigue still contribute to failure of most materials (Kamal and Rahman, 2018). Regardless of what has been mentioned in the latter, the catastrophic creep failures in the aerospace industry are now extremely rare due to the fact that creep and fatigue testing equipments have been designed such that they imitate real life loading for aircraft structures (Kamal and Rahman, 2018).

Farokhzadeh and Edrisy (2015) Defines creep as a time-dependent plastic deformation of a material under applied load, particularly at high temperatures. The driving force of creep is ascribed to the decrease in stress with time resulting in transformation from elastic strain to plastic strain. The rate and mechanism of creep in metals and alloys are related to the type of material, creep test time, temperature and the load (Liu et al., 2015). Creep deformation in metals and alloys is associated with dislocation generation, movement and annihilation. Temperature and grain size are the most dominant factors when determining the creep behavior

of a material. Nano-grained materials exhibit different creep behaviours when exposed to two different temperatures. At lower temperatures nano-grained alloy reflected high strength than at high temperatures (Zhao et al., 2018).

2.6.1. Creep stages

Conventionally, creep deformation is divided into three stages which are; primary, secondary and tertiary stages.

2.6.1.1. Primary stage of creep

During primary stage of creep the strain rate decreases with time until the steady secondary stage proceed (Yang et al., 2018). The primary stage of creep is mainly about competition between mechanisms of strain hardening and recovery. Initially, when the load is applied, there is an instantaneous straining and multiplication of dislocations which lead to an increase in density and subsequent work hardening. The deformation rate then decreases leading to rearrangement of dislocation with subsequent recovery which leads to steady state creep (Gollapudi et al., 2012).

2.6.1.2. Secondary and tertiary stages of creep

The secondary stage is the crucial and the longest stage of creep. It determines how long a material will last before it creeps. The longer the secondary stage of creep the shorter the survival of the crept material. Creep in this stage is independent of time. Meanwhile, in the tertiary stage, there is an increase in strain rate until the material creeps (Yang et al., 2018).

Figure 2.10 shows a typical conventional creep curve showing the three stages of creep.

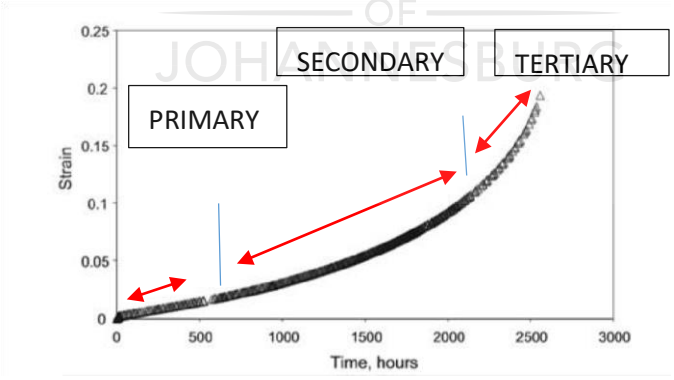

Figure 2. 10. Typical full creep curve showing three successive stages, namely: primary, secondary and tertiary stage (Abdallah et al., 2013).

Conversely, in nanoindentation creep, the lack of homogenous stress distribution on the sample during loading leads to inhomogeneous deformation. Therefore hardness is the only parameter used to measure the deformation behavior of a material (Yang et al., 2018). Figure 2.11 shows the indentation creep curve as a measure of indentation load against displacement.

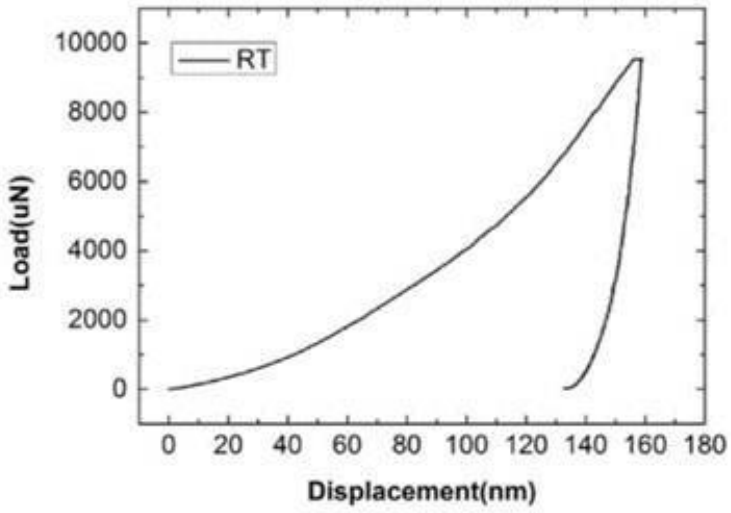

Figure 2. 11. Typical indentation creep curve of Load against displacement (Liu et al., 2012).

Gollapudi et al. (2012) reported that titanium alloys are ascribed to dislocation motion controlled creep at ambient temperature. It was observed that stresses lower than 50% of the yield strength can cause significant creep deformation in titanium alloys. Creep in this context was due to lower strain hardening ability of titanium at ambient temperature.

2.6.2. Mechanisms of creep

Creep can be classified into dislocation creep and diffusional creep mechanism. Dislocation creep is attributed to the power law behaviour and the diffusional creep is related to linear viscous behavior. The driving force of both mechanisms is related to diffusion and therefore follows the Arrhenius equation, as shown in equation 2.1(Badea et al., 2013). Basically, diffusion starts to occur when temperature is $0.3T_m$.

$$\varepsilon = A\sigma^n \exp(-\frac{Q}{RT}) \qquad \text{Equation 2.1}$$

2.6.2.1. Dislocation creep

It would be wise to understand that the stress that is needed to make a crystalline material deform plastically is the same stress needed to move dislocation from one point to another. So the stress would either be used to deform a material or move dislocation. The movement of dislocations can either be restricted by (a) lattice resistance or (b) the obstacles such as precipitates formed with undissolved atoms and dissolved atoms. Conversely, diffusion of atoms can unlock the dislocation movement under the applied stress and subsequently lead to dislocation creep (Ashby and Jones, 2012).

Figure 2.12. Shows how the movement of dislocation is hindered by the precipitates. The dislocation will not glide over until it hit the mid-plane of the precipitates. Analogous to the glide movement, the dislocation climb over is not possible due to the geometry. However, the

only way to allow the dislocation to climb over the precipitates was through the use of Fick's law of diffusion. The law states that the atoms will always move from the high concentration area to lower concentration area. The mechanical force is used to clear the atoms in an area of dislocation. In essence, creep is attributed the climb and glide of dislocation over the obstacles (Ashby and Jones, 2012).

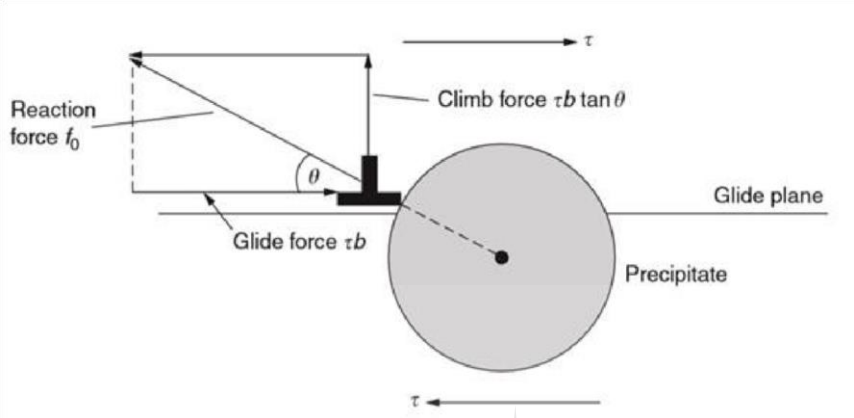

Figure 2. 12. Shows dislocation climb and precipitates hindrance (Ashby and Jones, 2012).

2.6.2.2. Diffusional creep

As the stress within the material decreases, the power-law creep becomes insignificant because the n value has to be between 3 and 8. Instead, another mode of creep emerges. When the stress σ is applied, the atoms diffuse from one face of the grain to another. Consequently, as the temperature goes high the diffusion of atoms occurs within the crystal, as demonstrated in Figure 2.13. At lower temperatures creep is attributed to grain boundary diffusion when stress is applied. To avoid vacancies between grains, grain boundary sliding occurs concurrently with grain boundary diffusion. Figure 2.14 and Figure 2.15 show a diagram of different creep mechanisms at given stress and temperature.

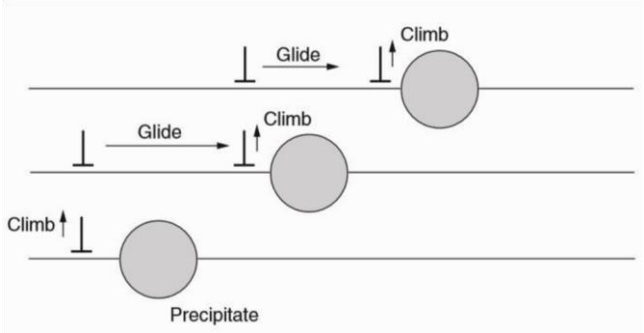

Figure 2. 13. Dislocation climb and glide movement (Ashby and Jones, 2012).

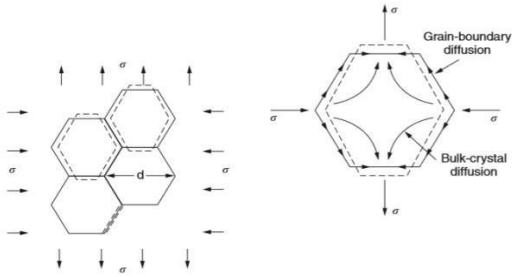

Figure 2. 14. Atoms diffusion along the grain boundaries (Ashby and Jones, 2012).

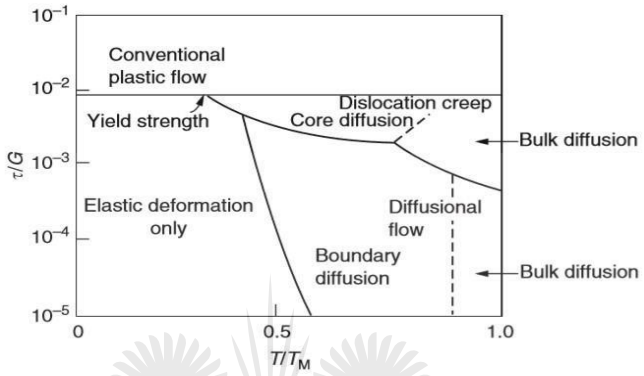

Figure 2. 15. Different mechanisms of creep (Ashby and Jones, 2012).

2.7 Factors affecting creep

2.7.1. Temperature

Temperature plays a paramount role on the creep phenomena of materials. Properties such as hardness, strength and microstructural arrangement are dependent on the temperature at which the material is exposed (Hu et al., 2018). Furthermore, as the temperature increases the material softens and all the work-hardening produced during plastic deformation gets counteracted by recovery process, subsequently creep occurs. The melting point of a material determines the temperature at which the material starts to creep. Generally creep occurs at $T > 0.3$ to $0.4\ T_m$ for metals and alloys, $T > 0.4$ to $0.5\ T_m$ for ceramics. Therefore, creep resistant material should feature high melting point (Hu et al., 2018).

Badea et al. (2013) investigated the creep behavior of Ti-6Al-4V alloys at 400^{o}C and 600^{o}C with the aim of understanding the effect of temperature and stress on the creep behavior of alloy. The Ti-6Al-4V alloy exhibited equiaxed microstructure with the alpha phase in lamellar matrix. First set of samples were tested at 400^{o}C and a yield strength of 480 MPa and the second set was tested at 600^{o}C and a yield stress of 330 MPa. It was reported that the specimens shows large creep deformation at 450^{o}C and 600^{o}C respectively. The SEM micrographs at 600^{o}C revealed ductile fracture surface characterized by pronounced necking and deeper voids. The

optical microscope images showed creep damage characterized cavities at the grain boundaries due to vacancy clustering were characterised by creep damage.

Meanwhile, Huang et al. (2017) investigated, the effect of Fe addition on the mechanical properties of alpha/beta titanium from ambient temperatures to 500^{o}C. It was reported that titanium alloys showed significant room temperature creep at stress below its yield strength. Creep became more pronounced when the temperature and stress increased. It was evident that at high temperatures and stresses, dislocations find it easy to move along the grains due to thermal activation. The ease with which dislocations move at high temperature consequently leads to diffusional creep, which occurs either by grain boundary sliding or coble diffusion. Movement of dislocations at lower temperatures is associated with planar slip, deformation twinning and stress induced martensite. Figure 2.16 shows the effect of temperature and stress on the creep resistance as time changes.

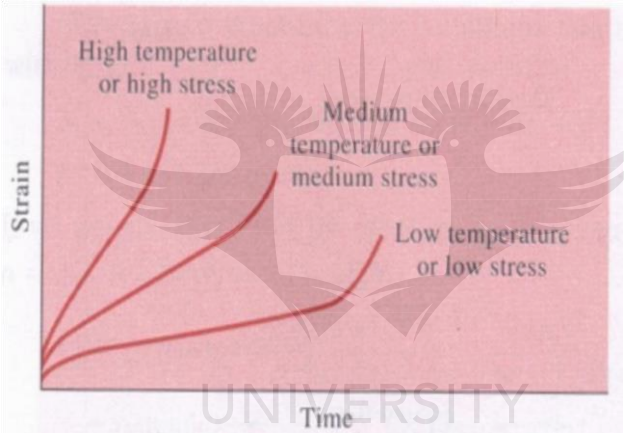

Figure 2. 16. Strain-Time curves demonstrating the dependence of creep deformation on stress (Reed-Hill et al., 1973).

2.7.2. Grain size

Grain size is one of the most important factor to consider when determining the creep behaviour of metals and alloys. According to Hall-Petch's, grain size play a paramount role in the strengthening mechanisms (work-hardening) as shown in the Equation 2.2 (Zhou et al., 2019).

$$\sigma_y = \sigma_0 + \frac{K_y}{\sqrt{d}} \qquad \text{Equation 2.2}$$

Where σ_y is the yield stress, $\boldsymbol{\sigma}_y$ resistance to dislocation of a material, K_y is a measure of dislocation pile up behind an obstacle, d is the grain size. According to Hall-Petch's relation decreasing the grain size should increase the strength of a material. Thence, the high amount of stress is required for continued deformation of a material. It can be inferred that materials with small grain size should be attributed to high creep resistance, while the materials with increased

grain size should exhibit low creep resistance properties. Lower creep resistance in larger grain size is attributed to a decrease in grain boundary area with a decrease in the number of grains resulting in less existing media to block dislocation movement (Zhou et al., 2019). On the contrary, when the grain is too small, due to high amount of stress and temperature it could possibly lead to other mechanisms of creep such as, grain boundary sliding, coble creep and grain rotation.

2.7.3. Crystallographic structure

Crystallographic structure of a material can be used to evaluate creep behavior of a material. Materials with HCP structure show significant creep at room temperature than BCC and FCC structures. Titanium alloys falls amongst this group of alloys with extended creep at room temperatures. Table 2.3 shows how Ti-6Al-4V alloy creep behaviour compares with other crystallographic structures. The n value determines the creep resistance of a material. At ambient temperature creep deformation occurs by dislocation creep through dislocation movement, or diffusional creep through atomic diffusion. The room temperature creep is attributed to dislocation activity, because 1) it occurs at low temperature where no diffusion can take place, 2) stress exponent has a value from 3 to 5 (n value depends on the alloy) (Sato et al., 2006).

Table 2. 3. Summary of creep parameters and evaluation of creep behavior of metals and alloys (Sato et al., 2006).

	Hexagonal (h.c.p.)				Cubic					
	c/a		Creep parameter					Creep Parameter		
	Material(primary slip system)	Material	N	E0.2/10^-8 s/1	Evaluation	Structure	Material	N	E0.2/10^-8 s/1	Evaluation
Metal	1.59 (prismatic)	CP-TiN	4.1	4.6	O	b.c.c	Pure Fe	-	-	X
	1.62 (basal)	Pure Zr	3.0	0.13	O					
		Pure Mg	4.7	10	O	f.c.c	1050Al	0.086	11	O

@:E0.2>10^-6 s/1 ,O:10^-6 s/1>E0.2>10^-9s/1 ,x:nil strain rate

2.7.4. Microstructure and nanoparticles

The influence of microstructure and nano-particles on the creep resistance is dependent on the creep mechanism. Analogous to the grain size, nanoparticles can improve the creep behavior of the material but does not have the same impact as the grain size. This is attributed to their relatively weak interfaces. Nanoparticles have the ability to prevent plastic flow, through the dislocation pinning effect, thereby increasing the strength and hardness of a material. Thus, high creep resistance is expected as the volume fraction of nanoparticles increases (Shen et al., 2013).

In their studies on the effect of microstructure on the creep response of Ti-6Al-4V alloys, (Briguente et al., 2012) reported that at constant load, at 600^{o}C and stress conditions of 125, 250 and 319 MPa respectively, bimodal microstructure specimen generated high creep resistance when compared to equiaxed microstructure see Figure 2.17. Figure 2.18 (a) and (b) show how creep test curves when temperature and stress are varied. It was observed that creep for both microstructures was dominated by the steady state creep

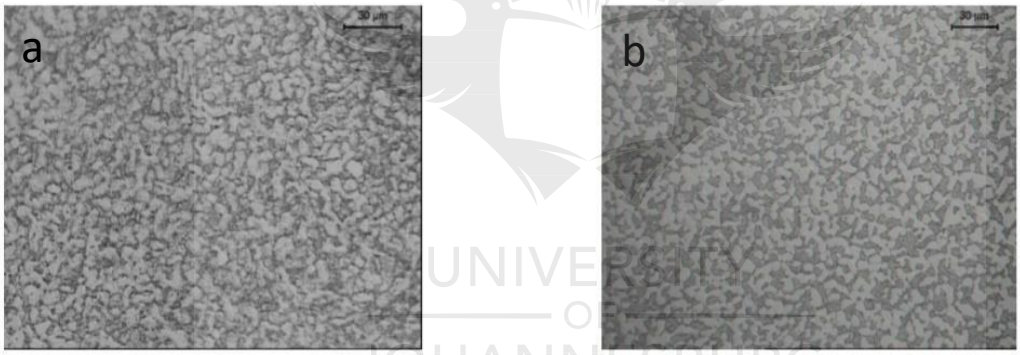

Figure 2. 17. Typical microstructure of Ti-6Al-4V (a) equiaxed (b) bimodal under cooling (Briguente et al., 2012).

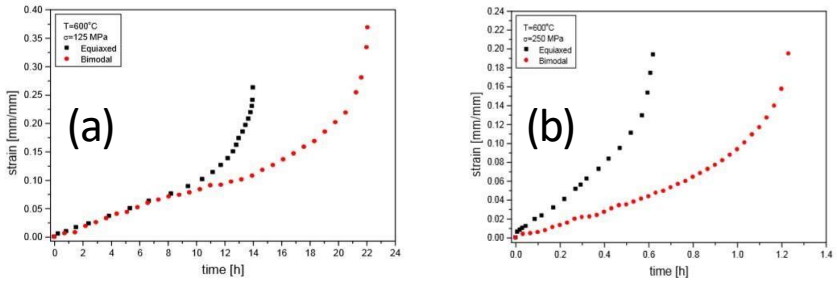

Figure 2. 18. Creep curves for equiaxed and bimodal at 600^{o}C (a) 125 MPa, (b) 250 MPa (Briguente et al., 2012).

2.7.5. Grain boundary

Zhang et al. (2016) evidenced that, grain boundaries are the main strong obstacles to hinder the dislocation motion. Grains are refined through the addition of second phase particles, precipitation hardening or incorporation of the nano grained materials and subsequently, grain boundaries are created. However, too many grain boundaries could lead to the embrittlement of the alloy as they act as strong dislocation motion. When the dislocations are hindered from moving along the obstacles they increase the stress around the obstacle and the overall internal stress of the material increases (Zhang et al., 2016).

2.7.6. Internal stress of the material

Generally, for creep to occur in metals and alloys the applied stress should exceed the internal stress of the material. Internal stress is associated with the stress field in the crystals of each and every material. The stress field in the material can either be long range or short range internal stress. Long stresses occur over a large scale whereas short range have to do with the short scale of stress. Bauschinger effect can be used to evidence the concept of long range internal stress. The material strain hardens and on reversal of the straining direction, the metal plastically flows at a lower stress than it was in the forward direction (Kassner, 2015).

2.8. Creep fracture

Fracture defined as a process of failure which occurs through three successive stages, which are crack nucleation, crack growth and rupture. Fracture normally occurs below the ultimate tensile strength in a crack free material. But as it is known, there is no perfect defect free materials. Materials are bound to have crack initiation sites arising from defects, inclusions and other foreign elements. There are two modes that define fracture, brittle and ductile fracture. Mode of fracture is dependent on the material type, the presence of pre-existing cracks, level of stress, temperature and environment (Mouritz, 2012).

2.8.1. Brittle fracture mode

Brittle fracture is characterized by little crack growth or plastic deformation in a material. It is mostly undesirable mode of fracture in the aerospace industry because it can lead to a complete failure of the material. It is sudden, catastrophic and occurs below the yield strength of a material. Brittle failure occurs with little or no plastic deformation at the crack tip. Once the applied load reaches the critical load for brittle crack to occur the material quickly propagates to failure (Mouritz, 2012). Therefore, it can be said that brittle fracture occurs only in two stages:

(i) Crack initiation normally at the pre-existing defect such as inclusions and voids; (ii) rapid propagation until failure. The fracture surface in brittle failure is defined by the presence of rock candy surface or cleavage type of fracture as in Figure 2.19 (Mouritz, 2012).

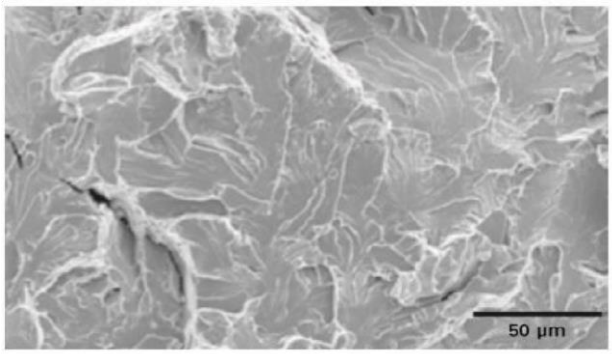

Figure 2. 19. Cleavage texture for a brittle surface (Mouritz, 2012).

2.8.2. Ductile fracture mode

Meanwhile, ductile fracture mode is defined by the presence of plastic deformation in a material at the crack tip. The crack continues to grow when the applied load is increased and ceases when the load is stable. The material can be saved from this mode of fracture because it gives warning and it is predictable. Hence, it is the most preferable mode of fracture. It is the dominant mode of fracture that occurs in aerospace industry in metals and polymer. Figure 2.20 shows how stress is distributed at the crack tip in metals as the applied stress increases. The applied stress is normally higher at the crack tip and reduces with distance from the tip (Polmear et al., 2017, Mouritz, 2012).

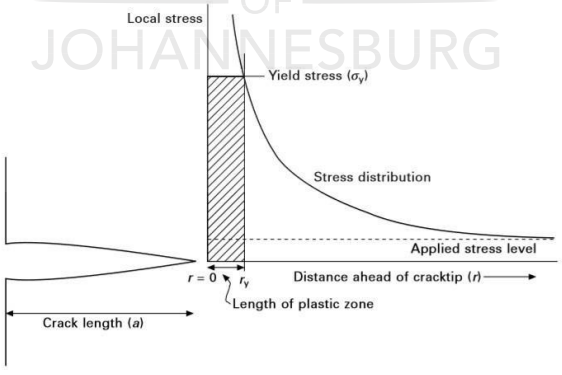

Figure 2. 20. Stress distribution at the crack tip in a ductile material under tensional loading (Polmear, 2001).

The extent of crack growth in a ductile material is a factor of the material type and the applied stress conditions. In many instances, high dislocation density in a plastic region which is a product dislocation interactions can lead to crack formation and growth. When the dislocations entangles and multiply at the main crack tip they turn to increase the stress at the crack tip resulting in the formation of minor cracks. Subsequently, the main crack and the minor cracks

produced from dislocations interconnect causing the advancement of the main crack and the crack is said to have propagated (Mouritz, 2012).

2.8.3. Transgranular and intergranular fracture

Fracture in material and alloys occurs either as transgranualr and intergranular. When the fracture occurs or propagate within the grains, it is called transgranular fracture. On the other, when it occurs between the grains it is called intergranular fracture. However, the combination of the two types of fracture can occur concurrently on a fractured surface. Intergranular fracture takes place where there is presence of hard brittle material located on the grain boundaries. The hard brittle particles thereby facilitate the crack growth on the grain boundaries (Dieter and Bacon, 1986). Figure 2.21 demonstrate pictorial diagram of how a crack propagates in and between the grains (Dieter and Bacon, 1986).

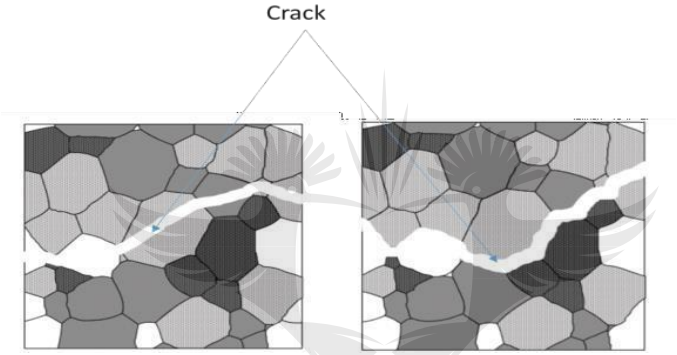

Figure 2. 21. Different mechanisms of fracture (a) transgranular (b) intergranular (Dieter and Bacon, 1986).

According to Polmear et al. (2017), the temperature at which the material is subjected to influences the texture of fracture. At lower temperatures the slip planes are weaker than the grain boundaries, thus transgranular fracture becomes dominant. Meanwhile, at high temperature grain boundaries are weaker than the slip planes and thus, intergranular fracture becomes dominant. Figure 2.22 shows how the texture surface change from cleavage to dimples as the temperature increases.

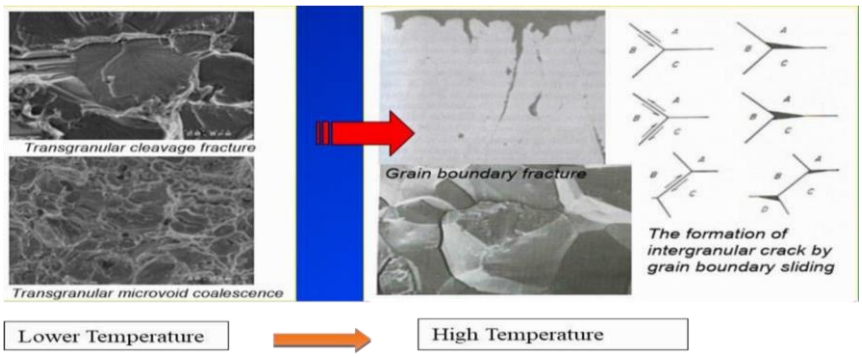

Figure 2. 22. Transition from Transgranular to intergranular (Polmear et al., 2017).

2.9. Wear Mechanisms

Wear is defined as a surface damage caused by a relative movement of solid particles past each other. Other studies, describe it as detachment of particles from the main substrate. It is attributed to either mass gain or mass loss depending on the wear mechanism. Wear behaviour is influenced by numerous factors such as the type of material, speed, angle of contact and the environment. Generally, lubricants are used to mitigate the wear problem. Lubricants work as the dividing fluid material that separates the contacting areas (Mphahlele, 2018).

There are lot of mechanisms which can be used to understand the phenomena of wear. Therefore, this work will focus on the most important mechanisms which are engineering related. Each mechanism of wear occurs in the form of fretting, erosion or impact depending on the intensity of contact. The categories are summarised below through the use of diagrams in Figure 2.23 (Kovaříková et al., 2009).

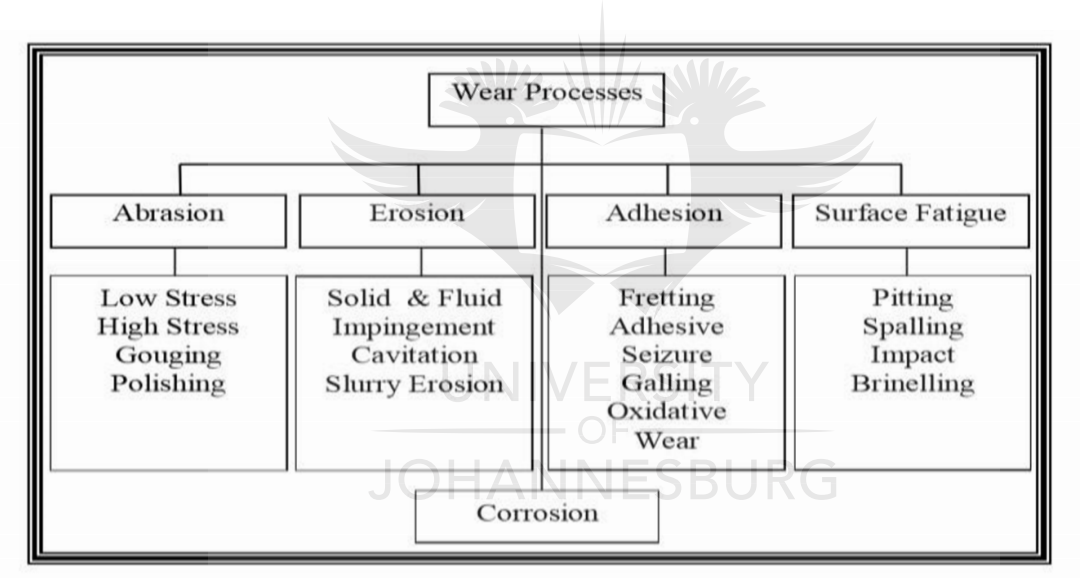

Figure 2. 23. Categories of wear (Bhushan and Gupta, 1991).

2.9.1. Adhesion

According to Stachowiak et al. (2006), adhesive wear occurs when two surfaces rub against each other in the absence of lubrication. This type of wear mechanism is normally referred to as sliding wear. The force needed to create the third surface is far less than the force needed to separate the two surfaces. Consequently, the third surface is created instead of separating the two contacting surface. Figure 2.24 shows typical diagram of how adhesive wear occurs. Adhesive wear is characterised by scuffing, galling, and gauging on the material surface (Stachowiak et al., 2006).

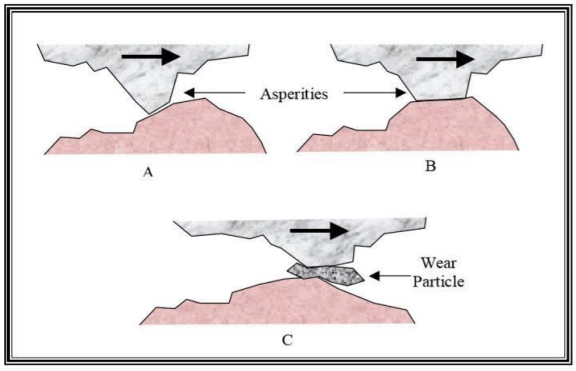

Figure 2. 24. Schematic diagram of adhesion wear (Stachowiak et al., 2006).

2.9.2. Erosion wear

Erosion wear also known as solid particle erosion is a type of wear mechanism that results when the hard erodent solid particle (A) impacts on the eroding solid surface (B) resulting in erosion of surface B as in Figure 2.25. The erosion wear rate depends on the process parameters such as the angle at which the A impact on B, velocity of the erodent laden fluid, size and shape of A and the temperature (Sharma et al., 2017, Stachowiak et al., 2006). To better understand the amount of material removed from the surface, the kinetic energy of the erodent particle is explained using Equation 2.3

$$\text{Mass od material removal} = \frac{K\rho MV^2}{2H} \qquad \text{Equation 2.3}$$

MV^2 is the kinetic energy of the erodent particle, ρ and H are the respective density and hardness of the erodent and K is the wear coefficient (Stachowiak et al., 2006).

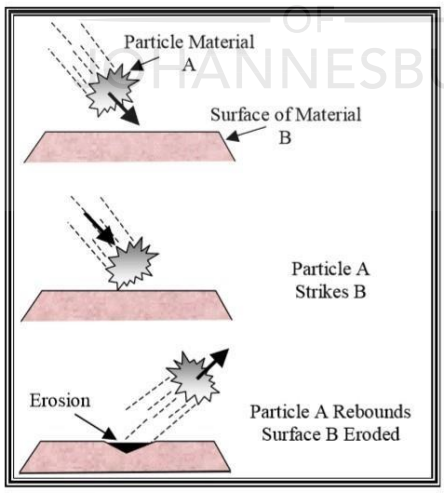

Figure 2. 25. Mechanism of erosion wear (Stachowiak et al., 2006).

2.9.3. Abrasion

Abrasive wear mechanism is a common type of wear which occurs when there is a material loss due to hard particles forcing each other against the surface. It is classified into two types which

are two-body contact abrasive wear and three-body contact abrasive wear. In a two-body contact wear there are two surfaces of which the softer surface gets eroded by an abrasive surface. This analogy is seen during grinding or cutting. Whereas, the three-body contact wear occurs when two sliding surfaces are embedded by an abrasive media (Mphahlele, 2018).

2.10. Testing methods

2.10.1 Nanoindentation test

Conventionally, the mechanical properties of material are tested at a macro and micro-scale. However, new techniques have been developed were the mechanical properties of materials can be studied at a nano-scale. The invention of new technologies such as nanoindentation testing allows one to test the mechanical properties of a material at a nano-scale (Mazeran et al., 2012).

Nanoindentation technique has emerged as a non-destructive method for testing the mechanical response of a material to applied load. It enables investigations of material under dynamic conditions which offer direct measurements of hardness, elastic modulus, creep and fatigue test of a material. This is done through the continuous recording of applied force and resulting depth penetration of the indenter through-out the loading and unloading cycle. Nanoindentation can continuously measure force and displacement as indentations are made without disrupting the microstructure. The parameters involved during indentation creep are maximum load, loading and unloading rate, temperature dwell time and contact pressure (Lucca et al., 2010).

Even though the nanoindentation technique can accurately measure the various continuous load and depth of a material up to a nano-scale. It is however dependent on various factors such as the indenter size, tip geometry and shape and also the strain hardening coefficient of the tested material which influence the pile-up and sink-in around the indenter tip (Gouldstone et al., 2000) . Factors that influence nanoindetation tests are discussed as follow:

2.10.1.1 Initial penetration depth

Generally, the initial penetration depth of the specimen is normally measured from the surface of the specimen without considering the effect of the indenter. In essence the initial displacement of the sample is measured in the absence of any external force. Instead, before the initial depth is measured the indenter should be in contact with the surface so that the initial overall depth can be measured before load is applied (Chen, 2009).

2.10.1.2 Tip geometry and Shape of the indenter

Mechanical testing methods require an indenter of a given shape and tip geometry to perform a special purpose. The commonly used indenters are Vickers, Rockwell, knoop and Brinell indenter, are characterized by 4D pyramid indenter and are mainly used in for micro and

macroindentation. Whereas, Berkovich and cube corner indenters are normally used at a nano-scale by virtue of their three-sided pyramidal geometry and small radii (Wheeler, 2009). Table 2.4 discusses different types of indenters used for indentation.

Table 2. 4. Different indenter types and their diameters (Wheeler, 2009).

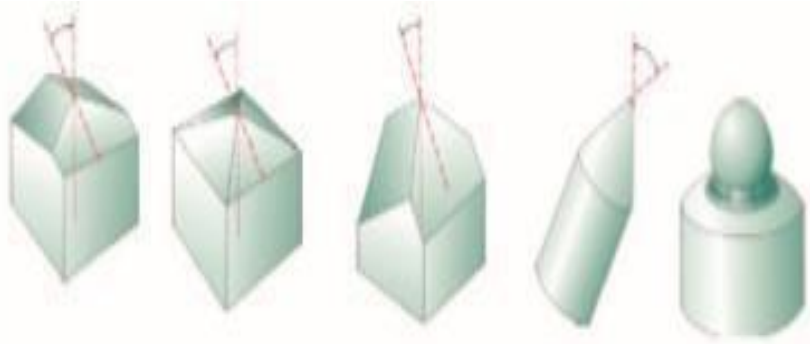

Features	Berkovich	Vickers	Cube – Corner	Cone (angle ψ)	Sphere (radius)
Shape	3-sided pyramid	4-sided pyramid	3-side pyramid/ perpendicular faces	Conical	Spherical
Applica-tions	Bulk materials, Thin films, Polymers, Scratch testing, Wear testing, Imaging	Bulk materials, Films and foils, Scratch testing, Wear testing	Thin films, Scratch testing, Fracture toughness, Wear testing, Imaging	Scratch testing, Wear testing, Imaging	Viscoelastic materials
Face angle, α	65.3°	68°	35.2644°	–	–
Area (projected)	$24.56h_c^2$	$24.504h_c^2$	$2.5981h_c^2$	πa^2	πa^2

However, according to Egart et al. (2016), the most recommendable indenter tip suitable for lot of practices is the berkovich indenter. Berkovich indenter is advantageous over other indenter tips owing to its unique properties such as:

- ✓ Uniformity of its shape which enables high accuracy
- ✓ Sharpness of the indenter tip which ranges in diameter of 20 nm
- ✓ Production of small plastic strains and hence less cracks after the test

2.10.1.3. Substrate of the tested material

Understanding the sample properties is relevant when testing the mechanical properties of a material at a nano-scale, thus dissipation of results is observed when probing a material of a heterogeneous surface (Egart et al., 2016). The substrate of the material tested plays a paramount role on the strain-hardening ability of a material and the response of the material to indentation. Ductile materials such as aluminium and copper are prone to pile-up at the indenter tip whereas brittle materials (ceramics and glasses) are susceptible to sink-in, as demonstrated in Figure 2.26. If a material experiences less strain-hardening during deformation, it is likely to cause pile-up at the indenter tip (Chen et al., 2006). Materials with high strain hardening coefficient have a likelihood of resisting deformation resulting in plastic deformation around the circle of the indenter and dissipate plastic deformation on the outer regions, this is referred as sink-in. Furthermore, when the deformation is increased the plastic zone extend to greater degree and sink in takes place (Chen et al., 2006).

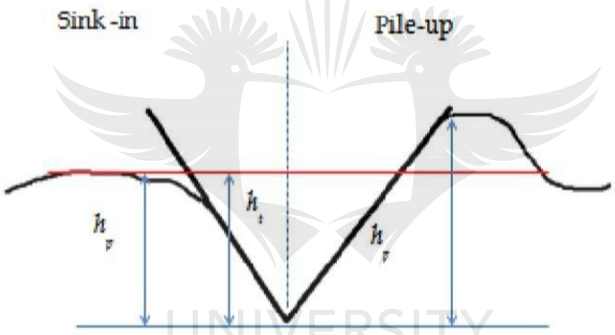

Figure 2. 26. Generic diagram of pile up and sink surfaces (Chen, 2009).

2.10.1.4. Thermal drift

Thermal drift is a common factor that affects nanoindetation tests results, particularly for test that are temperature sensitive. It is classified into two, the first of which is observed when the material experiences creep under plastic deformation. This kind is usually overlooked if the deformation volume is 0.1 % and below. The second one is seen when the material is subjected to constant load over a wide range of time, resulting in change in penetration depth. Consequently, depth penetration results could be erratic (Fischer-Cripps, 2011).

2.10.1.5. Extend of penetration depth

Size of penetration depth is dependent on the size, shape and the homogeneity or heterogeneity of the tested material. For the same volume of indentation, by the virtue of their shape, spherical indenter affect larger surface area and generates larger elastic strains under the indenter area as opposed to pyramidal indenters. On the other hand, the heterogeneity of a material can lead to varying penetration depth and hence low average depth due to conflicting mechanical response

of each alloy. As a result the resultant penetration depth is compromised and a highly alloyed composite can result in explicit inaccuracy (Králík and Němeček, 2014).

2.10.2. High temperature high velocity solid particle erosion test

Figure 2.27 shows a representative solid particle erosion test. Generally, the erodent particles of the required mass are fed into the hopper of the acceleration disc and pass through the channels in a rotating disc, resulting in a jet of particles ejected from the outlets of the tubes. The mass flow rate of erodent can be controlled and particle jets with different concentrations can be generated. The impact angle is adjusted by rotation of the sample with respect to the horizontal axis to avoid anomalies caused by possible rotation of erodent particles. The front edge of the sample is protected by a holder while the side edges are shielded by bracket to avoid intensive consumption of edges during testing (edge effect). In contrast to gas jet blasting type of devices, the collision of particles during impact and emerging of stagnation zones in centrifugal erosion tester with horizontal axis of samples rotation is reduced (Antonov et al., 2016). Factors influencing high temperature high velocity erosion test are discussed in following section.

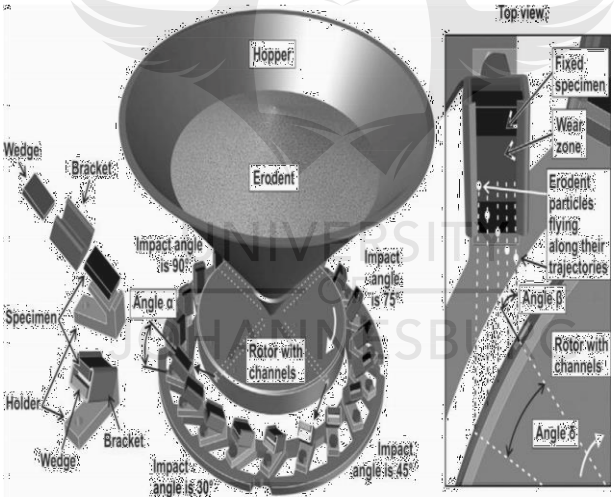

Figure 2. 27. High particle solid erosion test (Antonov et al., 2016).

2.10.2.1 Impact angle

One of the most important factors in erosion-wear is understanding the relationship between erosion rate and impact angle. An increase in erosion rate is observed from an impingement angle of 0^o and 45^o and then it reduces gradually at angles above 90^o (Sundararajan and Roy, 1997). For erosion to occur is imperative that the impact energy required for substance cracking is high enough to cause water delamination. At normal impact angles (90^o), there is larger contact area, which leads to plastic deformation. Lower impact angles (30^o), lead to shallow deterioration on the surface causing chipping with low cutting damage(Sharma et al., 2017).

However, works by Sundararajan and Roy (1997), argues that the influence of the impact angle depends on the material properties, ductile materials show high erosion rate at normal impact.

2.10.2.2 Impact velocity

The relationship between impact velocity and wear erosion is defined by the mathematical expression in Equation 2.4 (Kosa and Göksenli, 2017).

$$E_{wear} = K * v^{b} \quad \text{Equation 2.4}$$

Where, $E_{wear:}$ Wear rate, K: friction of coefficient constant, V: Impact velocity, B: powder index of velocity. The synergy between impact velocity, material hardness and erosion rate was investigated. An increase in wear rate was observed with high impact velocity and low hardness, as in Figure 2.28. On the other hand, wear rate was observed to be more pronounced on softer material at highest impact velocity (Kosa and Göksenli, 2017).

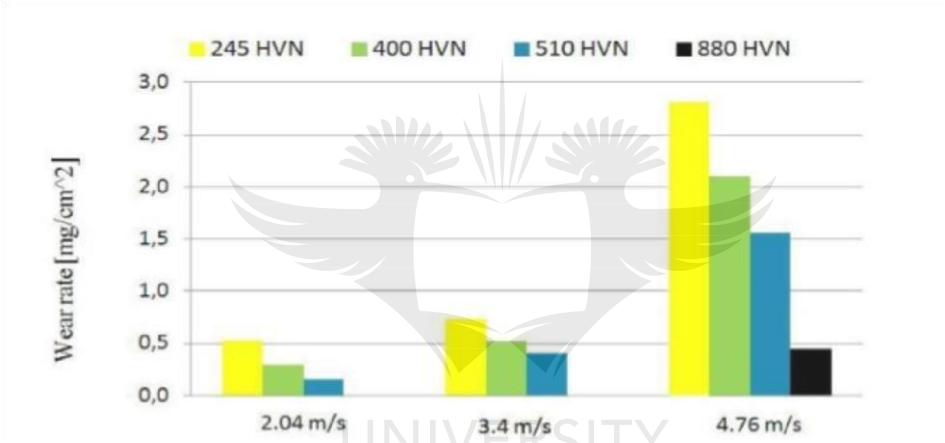

Figure 2. 28. Diagram of wear rate as a function of velocity and hardness (Kosa and Göksenli, 2017).

2.10.2.3. Particle size

Experiments have been conducted to compare the effect of particle size on the erosion response. Under the ideology that density and the velocity of the particles are the same, big particle sizes results in high erosion due to huge amount of kinetic energy they carry and transfer to the surface during impact (Akbarzadeh, 2010). Studies conducted by Sharma et al. (2017) revealed that increase with particle size has negative impact on erosion rate to a certain extend (up to 150um) and then a gradual decrease as the particle size got larger. U shape was observed with larger particle whereas w shape was noticed with smaller particle sizes. It was concluded that the larger particle sizes lead to a shorter life services of the components due to large contact area between the particle and the surface.

CHAPTER THREE: EXPERIMENTAL PROCEDURE

This chapter entails the experimental procedure executed in this work study. This includes the materials and methods used in the research study.

3.1. Mixing of feed Ti-6Al-4V-TiN powders

Ti-6Al-4V powders (APS 25 µm: Purity 99.9%) supplied by TLS-Technik, Germany and TiN powders (APS 20 nm: Purity 97%) supplied by Nanostructured & Amorphous Material Inc., Texas, USA were used as the starting materials. The Ti-6Al-4V and TiN powders of different compositions, as shown in Table 3.1, were loaded in a 250 ml cylindrical plastic vessel filled to 10% level, and further placed in the mixing chamber and subjected to translational and rotational motions for 8 h at a speed of 49 rpm. Spark plasma sintering (SPS) technology model HHPD 25 manufactured by FCT Germany was used for sintering the admixed powders. Spark plasma sintering technology generates high sintering speed. In SPS technology, the raw powder is loaded into the graphite die vertical pressure and a pulsed electric current voltage is passed through the die. The sintering temperature is monitored using thermocouple for temperatures below 1000˚C and a pyrometer for temperatures above 1000˚C. The optimized SPS parameters used were: pressure of 55 MPa, temperature of 1100ºC, heating rate of 100ºC /min and holding time of 30 minutes.Ti-6Al-4V+TiN composites with die dimensions of 40 mm diameter and 5mm thickness were produced. Optical microscope, SEM and XRD were used respectively to analyse the microstructural evolutions and phases present.

Table 3. 1. Compositions of mixed powders

S/N	Ti-6Al-4V alloy (wt. %)	TiN (wt. %)
1	100	0
	98	2
2		
3	96	4
4	94	6

3.2. Relative density measurement

Spark plasma sintered samples were sand-blast to remove the alpha-case due to graphite die carbon pick-up in sintering. Thereafter, Archimedes density kit was used to measure the density of the samples. Archimedes density method can accurately weigh and measure the density of the liquids and solid. The samples were weighed five times for accuracy, the average values

were calculated and recorded as the final density of the samples. Lastly, the recorded densities were used in Equation 3.1 to determine the theoretical densities of the sintered samples. The relative density of the samples was then determined by dividing measured density by theoretical density.

$$\text{Theoretical density} = \frac{(100)}{\left(\frac{w\%A}{PA}\right)+\left(\frac{W\%B}{PB}\right)} \qquad \text{Equation 3-1}$$

Where, A and B in Equation 3.1 above represent individual elements present in the alloy compositions. The relative density was obtained by diving measured density with theoretical density.

3.3. Surface preparation: grinding and polishing

The sintered samples were cut using the Brillant 220 automatic precision cut off saw machine made in Germany .The cross-section was grinded and polished using the SAPHIR 550 grinding and polishing machine to produce a mirror like surface. The 320 grit SiC grinding paper was used for rough grinding of the surface. For initial and final polishing stages, Aka-Allegran 3 polishing pad with Dia-Maxx 6 microns' poly suspension and Aka-Chemal polishing pad with Fumed silica 0.2 microns were used respectively. The samples were grinded at a speed of 300 revolutions per minute (rpm) until a flat surface was obtained, then the first and second stage of polishing were done at a speed of 150 rpm. The polished surface was etched with kroll's reagent (92 ml distilled water, 6 ml Nitric acid and 2 ml Hydrofluoric acid) for 30 seconds subsequently rinsed in pure water, air dried water at least ten minutes to prepare the samples for hardness testing and microstructural characterizations.

3.4. Microstructural characterization of the sintered samples

The prepared samples were analysed for metallographic analysis and mechanical properties. The following techniques were used for the metallographic and chemical analysis characterization: optical microscope, scanning electron microscopy and X-ray diffraction. Consequently, the mechanical properties were evaluated using: Vickers hardness tester, Ultranano-indentation and high temperature high velocity solid particle erosion tester.

3.4.1. Optical microscope (OM) and Scanning electron microscopy (SEM)

Spark plasma sintered Ti6Al4V+TiN composites were examined for microstructural evolution, morphology, grain size and topography using SEM (JEOL JSM-7600F) and Optical microscope. EDS was used to analyse the elements present in the composites after sintering.

3.4.2. X-ray diffractomer

X-ray diffraction of polished surface of sintered specimen was conducted on a PANalytical Empyrian diffractometer using monochromatic Cu Kα radiation at a tension of 40 KV and 30

mA. The XRD analysis was done to identify the phases present in the powders as well as in the sintered specimen. A scanning step mode of 0.02 was used during X-ray diffraction. Diffract grams were collected over a 2θ range between 5 to 90^{o} at room temperature. High Score Plus software was used for identification of the constituent phases.

3.4.3. Vickers hardness tester

Vickers hardness tester (Innova Test Falcon 500) was used to measure the micro-hardness of the polished surface of SPS samples. The load of 100 gf and dwell time of 15 seconds were used. Five indents were made randomly on the sample and the average hardness was used for accuracy of the results.

3.4.4. Nanoindentation creep tests

The sintered specimen of Ti-6Al-4V+TiN of dimensions 40 mm diameter and 2.5 mm thickness was used for this test. The Ti-6Al-4V alloy and Ti-6Al-4V + TiN alloys with volume fractions of 2, 4 and 6% TiN were used to study creep at room temperature (25 ^{o}C) and the effect of thermal drift were taken into consideration. Room temperature Creep tests were conducted using ultra-nanoindentation technique (UNHT Anton Paar ,Switzerland), as shown in Figure 3.1. The test is equipped with the Berkovich indenter, which is calibrated, to maintain accuracy during the tests.

The indentation tests were performed at 3 different loads which are 40 mN, 60 mN and 100 mN respectively. For each applied load, the loading and unloading rates were set to be 20 mN/min with varied holding times of 100 s and 200 s, respectively. Each indentation test was repeated 3 times and 18 indentations for each loading and unloading experiments were performed on randomly selected areas on each composite. The indents were located 30 µm apart to avoid the influence of residual stress from the adjacent impressions. Each indentation cycle consisted of four steps, loading to maximum applied load, holding at maximum load, unloading to 10 % of the maximum load for recovery purposes and holding at a minimum. The nanoindentation creep was calculated through the data provided by the software.

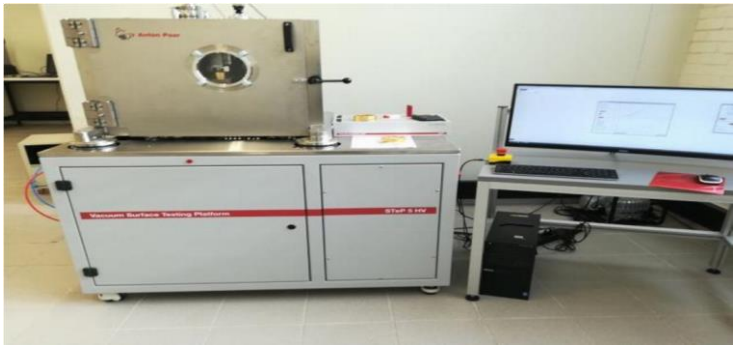

Figure 3. 1. Ultra-nanoindentation tester

3.4.5. High velocity erosion testing

The Ti-6Al-4V alloy and Ti-6Al-4V+TiN with volume fractions of 2, 4 and 6% TiN were used to study erosion-wear behavior at room temperature (25^{o}C). Alumina was used as an erodent particle. Firstly, the erosion tests were performed at 4 different times which are 2 min, 5 min, 8 min, and 10 min, respectively, at an incident angle of 90^{o} and particle velocity of 20 m/s. Meanwhile, each test was conducted five (5) times on the samples to achieve results of high accuracy. Additionally, the Mass loss and the average wear depth and wear morphology of the sintered samples were evaluated. Wear tracks and wear depth were evaluated using SEM and Confocal microscopy. Optical microscope was used to analyse the microstructure and XRD analysis was used to identify if there were any formed phases from the erosion test..

3.4.6. Ball on disc tribometer

The ball on disc experiments were conducted on the Ti-6Al-4V+TiN composites to evaluate the wear properties. The tests were performed at room temperature at a normal force of 5N and radius of 6mm. Each experiment was conducted at a rotational speed of 5.06 cm/s for 30 minutes, and a steel ball of 6 mm was used as the erodent particle.

CHAPTER FOUR: RESULTS AND DISCUSSIONS

In this section, the microstructure, erosion-wear properties, wear, elastic and plastic properties of spark plasma sintered Ti-6Al-4V and Ti-6Al-4V+TiN were presented and discussed. Microstructural analysis of the sintered samples was done using optical microscope and scanning electron microscope, while, X-ray diffraction was used for phase identification. The mechanical tests carried out were investigated using high velocity erosion test, ball on disc tribometer and ultra-nano indentation test.

4.1. Microstructural characteristics

The optical and scanning electron microscopy (SEM) images of spark plasma sintered Ti-6Al4V alloy and Ti-6Al-4V+TiN of fractions 2 w%,4w% and 6w% are shown in Figures 4.1 and 4.2 respectively. The microstructure is a function of spark plasma sintering process parameters and chemical composition of the powders (Mphahlele, 2018, Veiga et al., 2012). It was evidenced that as the presence of TiN nanoparticles increased from 2w% to 6w%, microstructural transformation took place from lamellar microstructure in Figure 4.1 (a) to a bimodal microstructure in (b). TiN particles inhibits grain growth through pinning grain boundary migration (Russias et al,.2005).

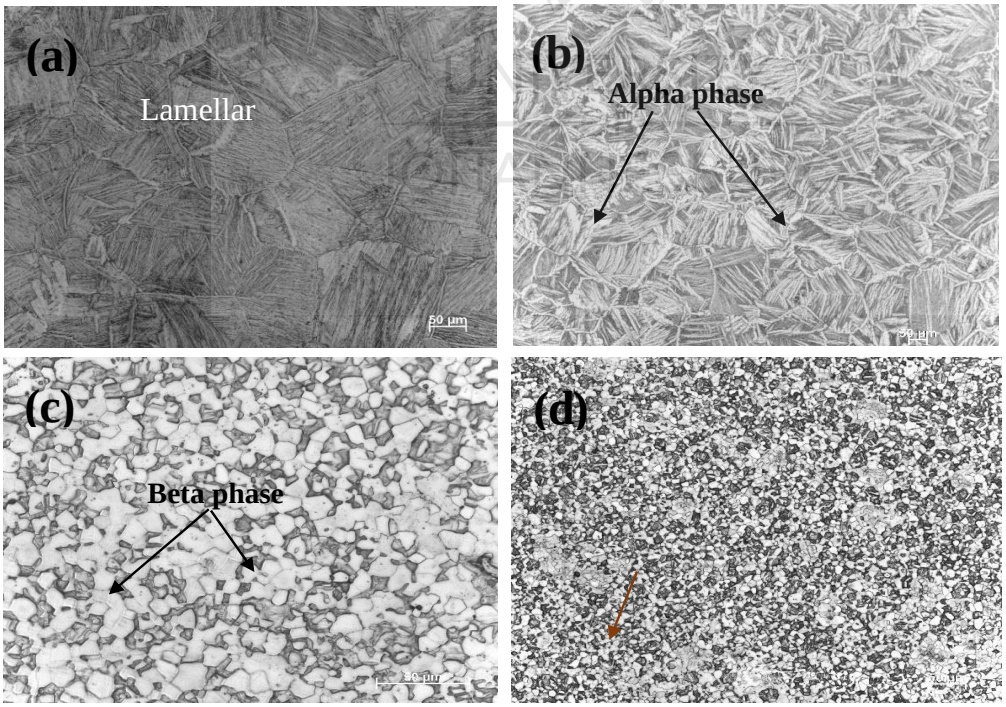

Figure 4. 1.Optical microstructures showing the effect of TiN on the microstructure of Ti-6Al-4V

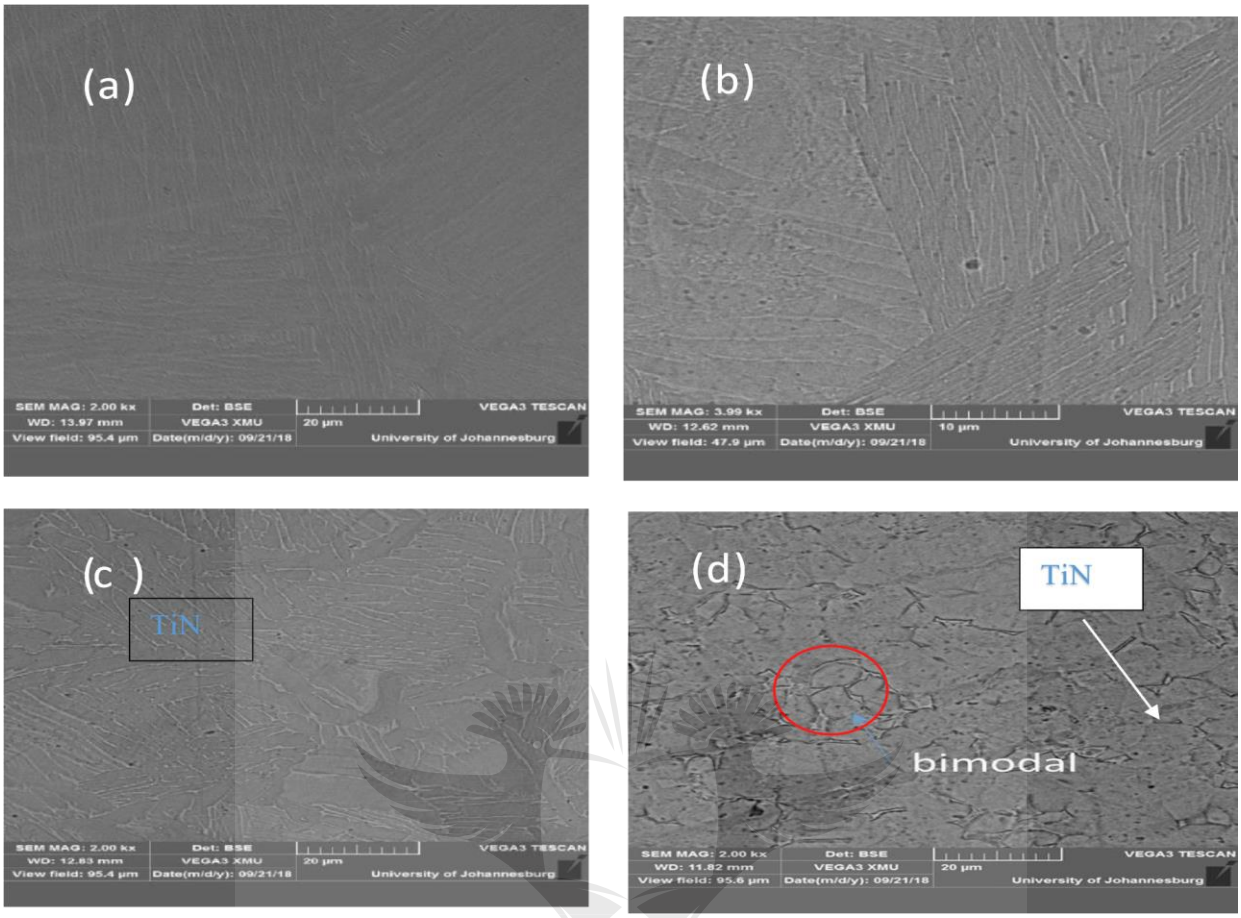

Figure 4. 2. SEM micrographs of (a) Ti-6Al-4V (b) Ti-6Al-4V+2TiN (c) Ti-6Al-4V+4TiN (d) Ti-6Al-4V+6TiN

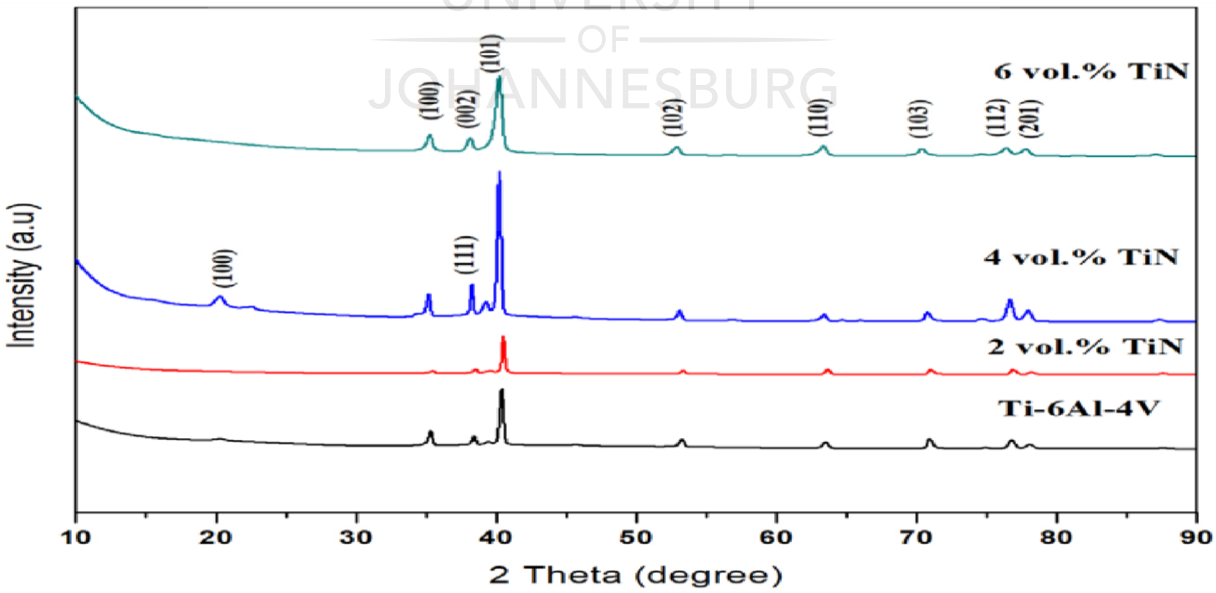

Figure 4. 3. XRD diffractographs of Ti-6Al-4V alloy and Ti-6Al-4V+TiN (2, 4 and 6w %)

XRD diffraction patterns of SPS Ti-6Al-4V alloy and Ti-6Al-4V +TiN are presented in Figure 4.3. The diffraction peaks increased from lower intensity to high intensity with an increase in TiN content. The presence TiN increased the alpha phase in the microstructure, hence broader diffraction peaks are observed as TiN content increases. However, it was noticed that the intensity of the alpha and beta diffraction peaks reduced as TiN content goes to 6 vol.%.This could be attributed to lack of homogeneity in the TiN and Ti-6Al-4V powders during mixing. The presence of TiN in the spark plasma sintered Ti-6Al-4V is characterised by the reflections (110), (111) and (221) at peak positions 2θ=3.52°, 39.3° and 60.8° respectively.

4.2. Mechanical properties

The increasing use of engineering materials in severe environments requires a material that exhibits good mechanical properties (Lucca et al., 2010). Understanding the mechanical properties of an alloy assist one to select a perfect material for an intended application; most importantly it enriches user's mind of the behavior of material, quality, and assist in selecting an economically friendly and cost effective alloy. Therefore, metallic materials are used in design of most components and structures owing to their mechanical properties such as the ability to withstand high service loads (Carrion et al., 2017).

4.2.1 Erosion-wear properties

4.2.1.1 Mass loss

In section, the erosion-wear behaviour of Ti-6Al-4V+TiN composite was evaluated as a function of mass loss against TiN volume fraction. The bar graph in Figure 4.4 presents the average mass loss of Ti-6Al-4V and Ti-6Al-4V+TiN for different test times. On increasing the TiN content to 2 wt%, the mass loss reduced significantly but tend to increase when TiN increased to 4wt%. Further increase in TiN content to 6 wt% reduced the average mass loss. The increase in average mass loss at 4 w% TiN may be due to agglomeration, lack of homogeneity and inclusions. The mass loss in Ti-6Al-4V was lower than the composite, which is an indication that TiN addition improved wear resistance. In the comparative study conducted by Mphahlele (2018), an increase in TiN nanoparticles upto 6 wt% revealed an improved wear properties and a reduction in wear properties was reported at 8 wt%. Russias et al. (2005) reported an increase in hardness and wear properties at 6 wt% TiN addition.

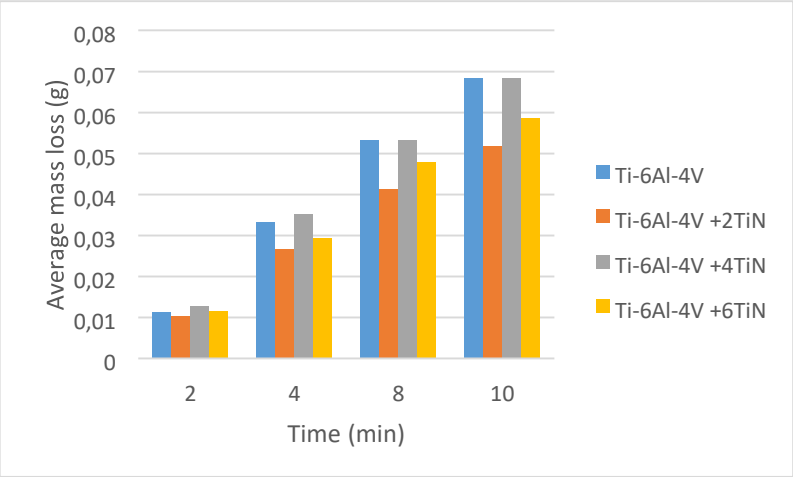

Figure 4. 4. Weight loss of the sintered Ti-6Al-4V + TiN composite

Figures 4.5 and 4.6 show macro-morphology of the eroded surfaces of Ti-6Al-4V+TiN composites after 10 min. The macromophology of the eroded surfaces revealed the presence of pits and inclusions on all the composites. The presence of defects and inclusions can act weakening sites resulting in reduced mechanical response. The estimated final erosion diameter of Ti-6Al4V alloy was 11.63 mm. In comparison to Ti-6Al-4V alloy, when the TiN content increased to 2 wt%, the diameter reduced to 8.20mm. Subsequently, the diameter of the eroded surface expands to 10.51 mm at Ti-6Al-4V+4 w% TiN then reduces to 9.8 mm at Ti-6Al-4V+ wt6% TiN.

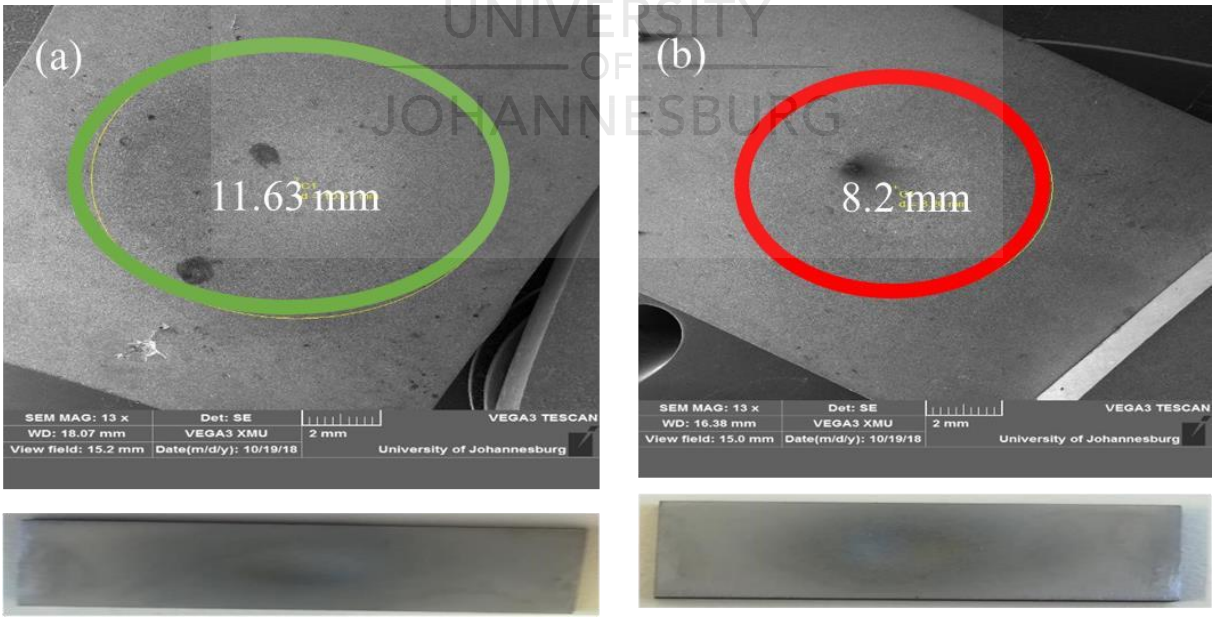

Figure 4. 5. SEM micrographs of eroded surfaces of (a) Ti-6Al-4V (b) Ti-6Al-4V+2TiN at test parameters: 10min, 90^{o} incident angle.

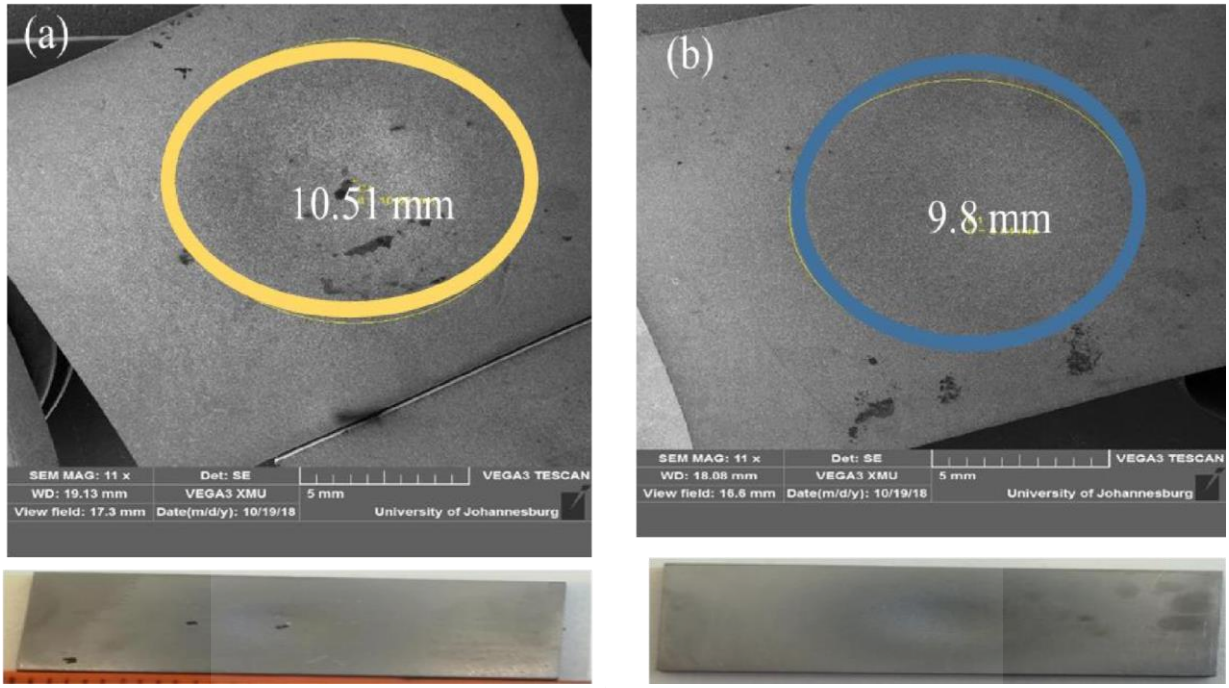

Figure 4. 6. SEM micrographs of eroded surfaces of (a) Ti-6Al-4V+ 4TiN (b) Ti-6Al-4V+6TiN at test parameters: 10min, 90^{o} incident angle

4.2.1.2 SEM and confocal images

Confocal microscope and SEM erosion-wear micrographs of Ti-6Al-4V + TiN composites are displayed in Figures 4.7, 4.8, 4.9 and 4.10. On the confocal mapping the blue colour represent the maximum depth at which erosion has taken place and the red colour shows the minimum surface on which erosion has taken place. It was observed from the colour coding, that erosion was dominant at the center (blue) of the surface and yielded slowly outward the surface (red). Furthermore, Ti-6Al-4V alloy presented the greatest confocal mapping depth of 974.721μm, this indicate high erosion depth. Ti-6Al-4V+2TiN revealed a depth of 933.361 μm, indicating minimum erosion of the composite.

However, erosion depth tend to increase when the TiN content increased to 4 wt%. Further, at 6 wt% TiN, erosion depth decreased again. SEM micrograph Figure 4.7 (a) Ti-6Al-4V alloy shows the presence of micro-pits, which resulted from gouging of the surface by the erodent surface. It can be concluded that the presence of TiN improved the wear properties of Ti-6Al-4V. Fundamentally as the fraction of the nanoparticles increases the strengthening effect should increase (Yu et al., 2019).

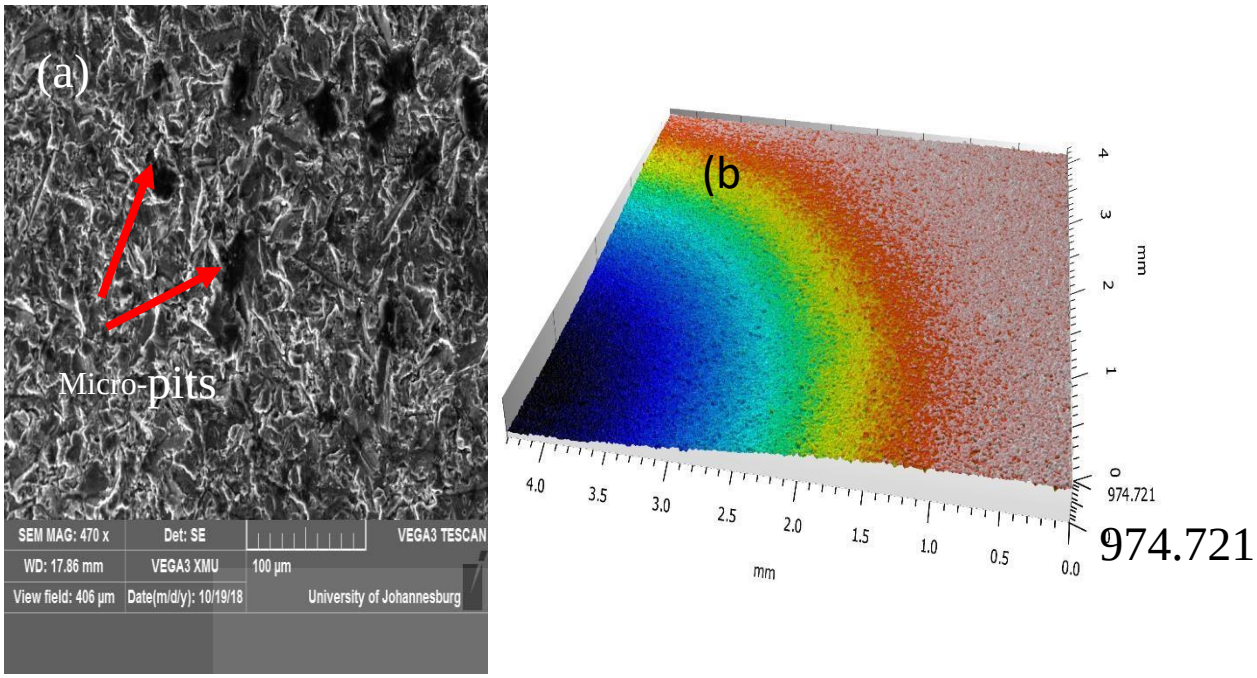

Figure 4. 7 Ti-6Al-4V alloy erosion SEM micrographs (a) with corresponding confocal image (b)

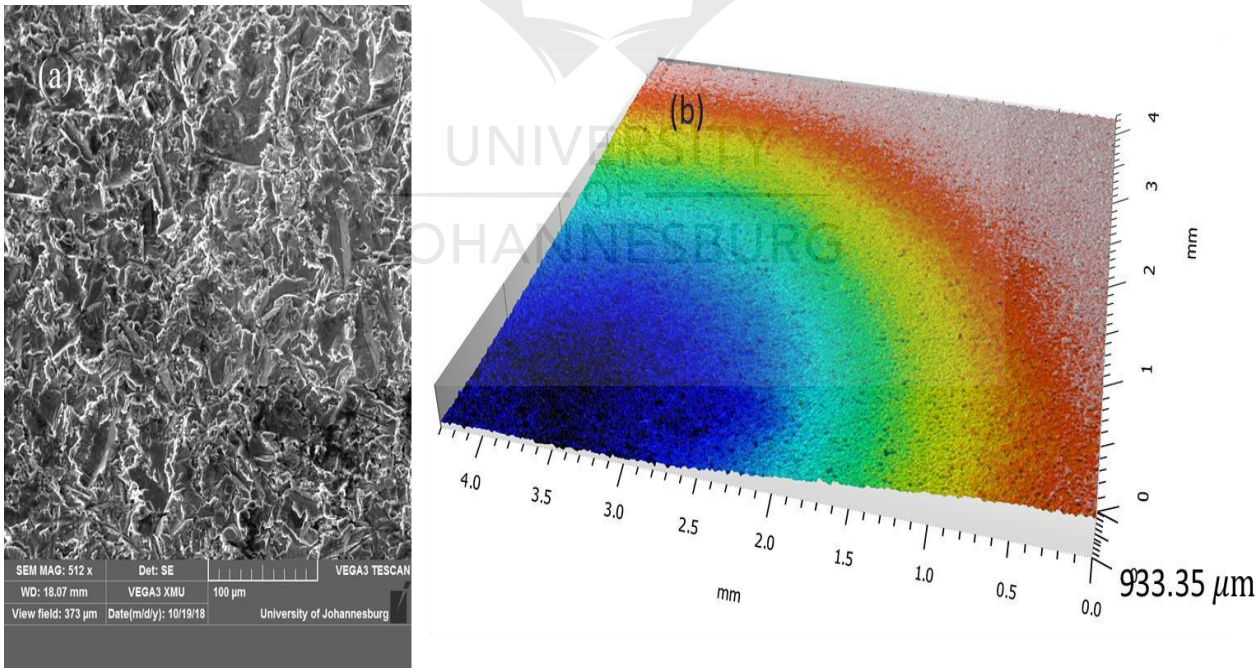

Figure 4. 8 Ti-6Al-4V + 2TiN alloy erosion SEM micrographs (a) with corresponding confocal image (b)

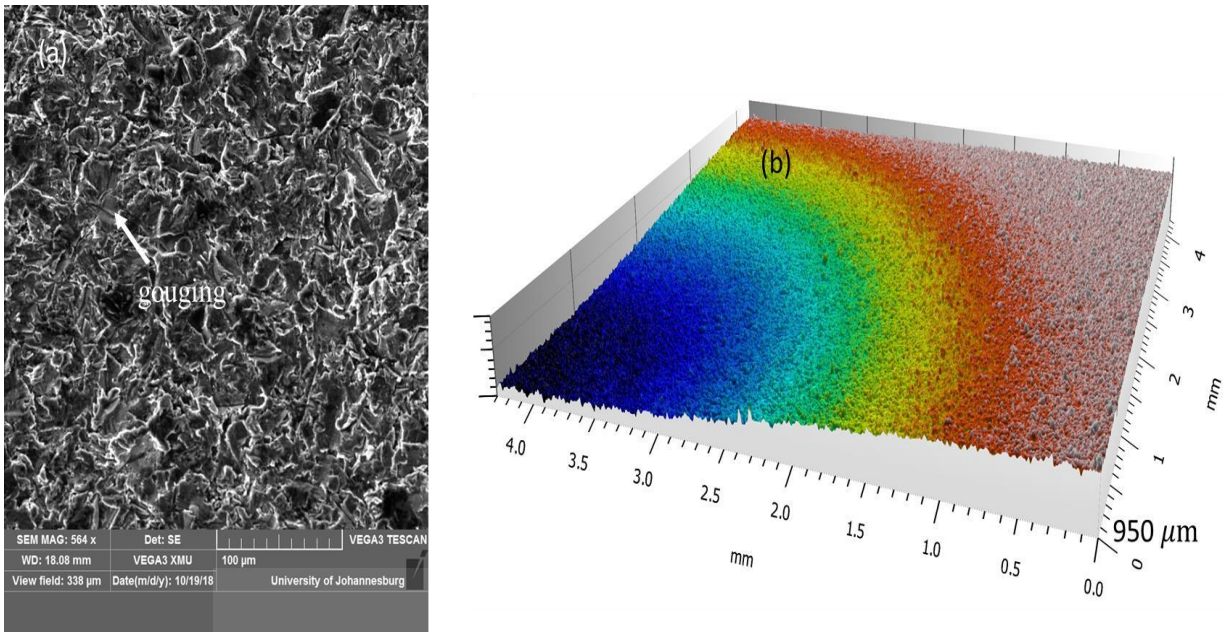

Figure 4. 9. Ti-6Al-4V + 4TiN alloy erosion SEM micrographs (a) with corresponding confocal image (b)

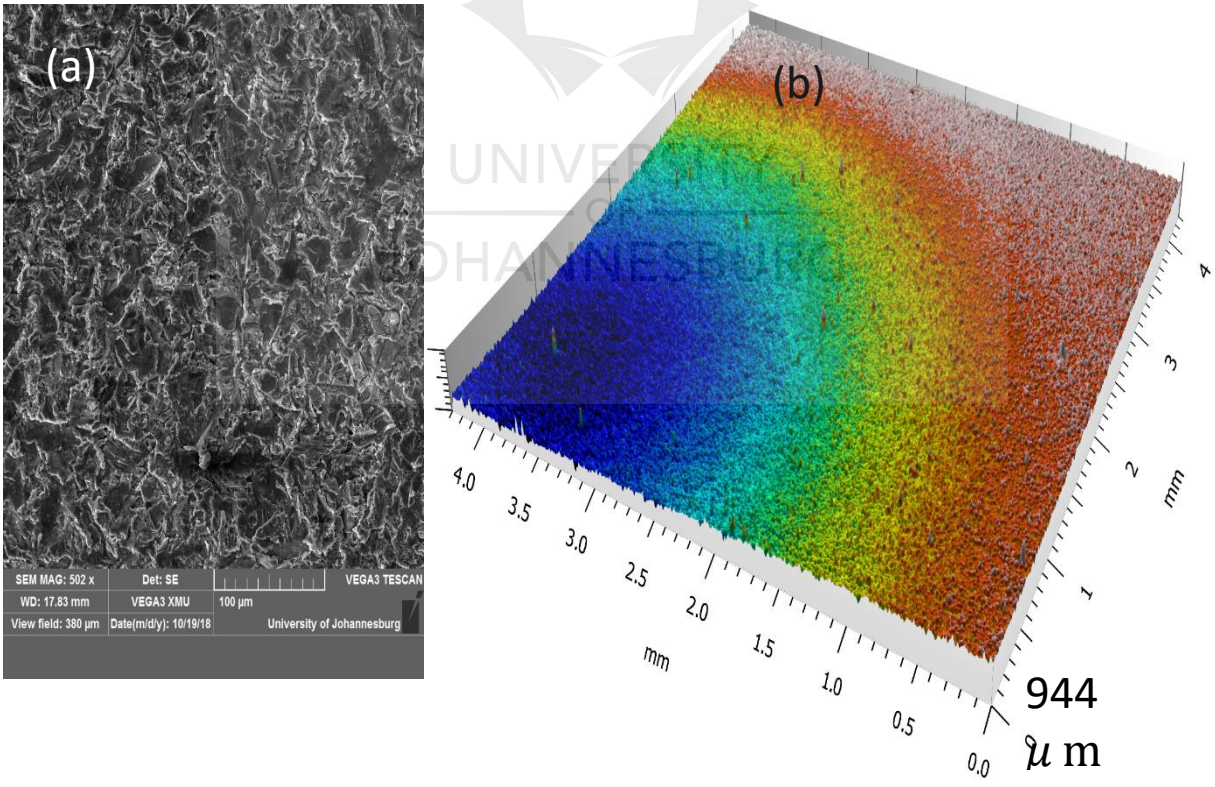

Figure 4. 10. Ti-6Al-4V + 6TiN alloy erosion SEM micrographs (a) with corresponding confocal image (b)

4.2.2 Wear and friction properties

4.2.2.1 Wear

The bar graph of average mass loss as a function of composites is shown in Figure 4.11. Ti-6Al-4V alloy exhibited the highest mass loss. On increasing TiN content to 2 wt%, the average mass loss of the composite reduced significantly. However, the average mass loss tended to increase with an increase in TiN content to 4 wt%. The lack of strengthening effect in TiN at 4 wt% when compared to 2 wt% was attributed to the aggregation of the nano particles and degradation in refinement which leads to grain boundary sliding (limitation to hall patch), hence high wear rate (Yu et al., 2019). At 6w% TiN the average mass loss has shown a decrease. This may be due to the strengthening effect of TiN on the matrix of Ti-6Al-4V through the Orowan strengthening theory. In addition, the overall mass loss of Ti-6Al-4V alloy increased with an increase in TiN reinforcement.

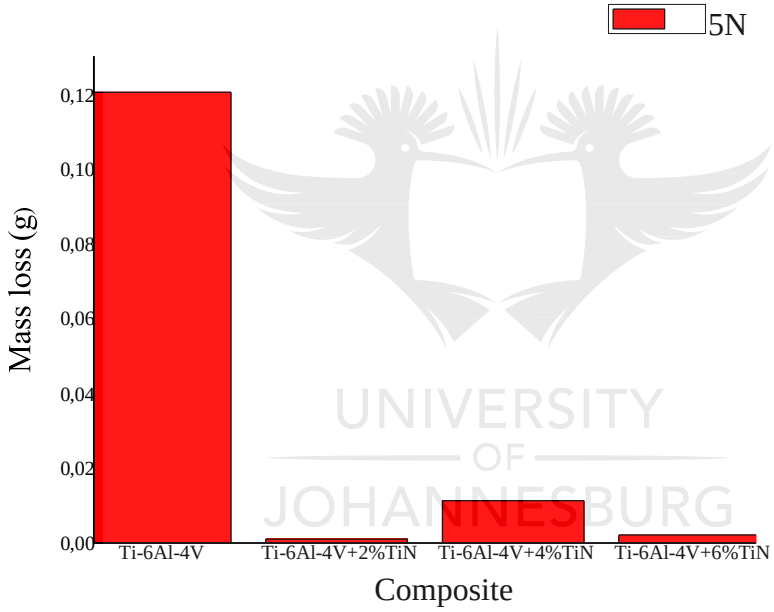

Figure 4. 11. Average mass loss against Ti-6Al-4V+TiN composites

4.3.2. Coefficient of friction /

Figure 4.12 below explains wear behaviour as a function of average coefficient friction against TiN contents. It was clear that the friction coefficient of Ti-6Al-4V alloy increased significantly as TiN contents increased from 2 wt%. On the other hand, when TiN content was increased to 4 wt% the friction coefficient decreased. This could also be explained by the high percentage mass loss that occurred in Ti-6Al-4V+4TiN when compared to other composites. The increase in the overall coefficient of friction could be attributed to the presence of hard TiN nanoparticles in the matrix, which are pulled out during contact. Nanoparticles have the ability to prevent plastic flow, through the dislocation pinning effect, thereby increasing the strength and hardness

of a material. Thus, high wear resistance is expected as the volume fraction of nanoparticles increases (Shen et al., 2013). It could be deduced that the increase in TiN addition improved the wear resistant of Ti-6Al-4V alloy.

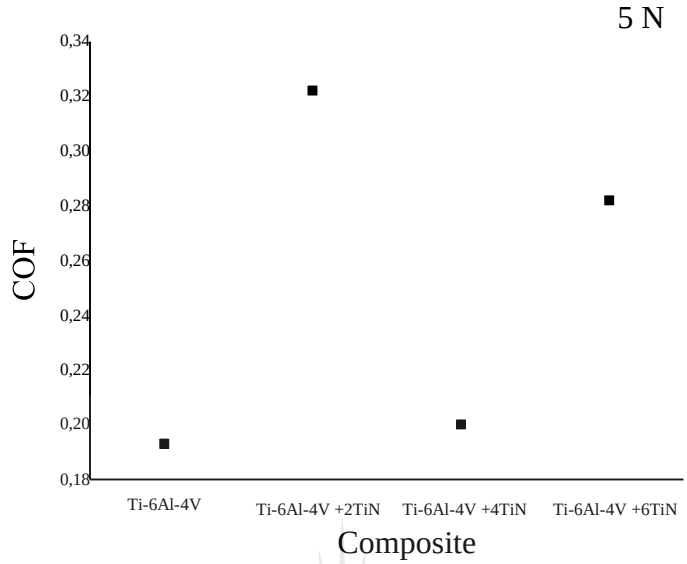

Figure 4. 12. Mean value of coefficient of friction of Ti-6Al-4V alloy and its composites. Mean values were obtained from the total test duration

4.2.3 Macro hardness properties in correlation to nano hardness properties

Results of nano hardness and Vickers hardness are presented in Figure 4.13. The addition of TiN reinforcement from 0 wt% to 2 wt % increased the hardness properties of Ti-6Al-4V alloy by 5%. Furthermore, a reduction in hardness by 10% was observed at 4wt% TiN addition. On the other hand, 6wt% TiN addition revealed an increase in hardness by 17%. It could be seen that the hardness values follow the same trend both in nano hardness and micro hardness results.

In both cases Ti-6Al-4V alloy displayed lower hardness properties of 342, 6 HVN and 3308 MPa. Conversely, Ti-6Al-4V+2 wt% TiN and 6 wt% TiN presented high hardness values of 388,3 HVN and 372 HVN and 7112,3 MPa and 4292 MPa Vickers and nanohardness values respectively. Moreover, it was noted that nanohardness values were significantly high than the vickers hardness values. This was due to the fact that, the nano hardness results were taken at a nano scale, enabling indentation on hard TiN nano particles. It could be argued that an increase with hardness was attributed to the presence of strong hard TiN nanoparticles on the grain boundaries. Due to their pinning effect, nanoparticles have the ability to prevent plastic flow, consequently increasing the strength and hardness of a material.

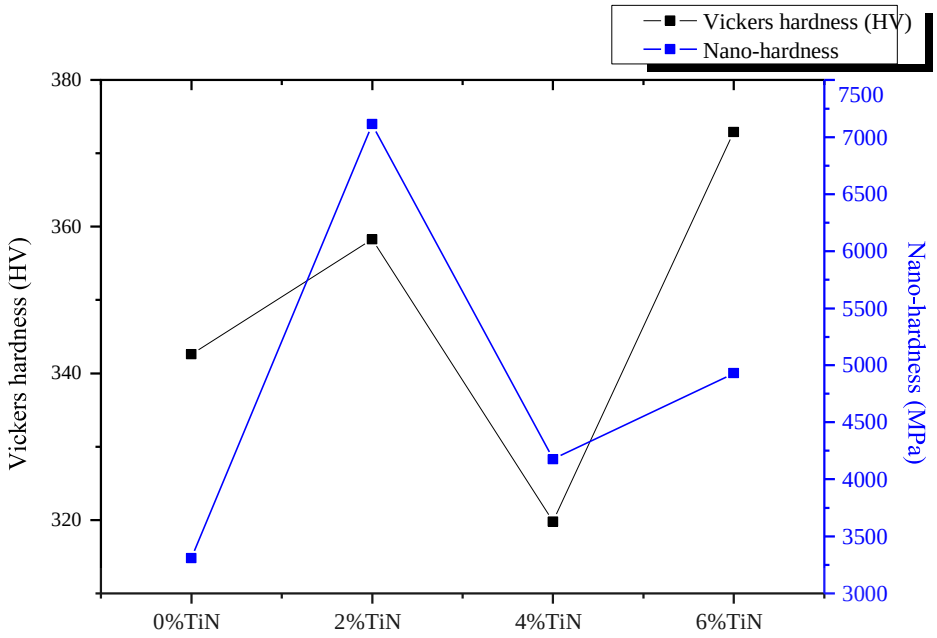

Figure 4. 13. Average Vickers hardness and nanohardness of Ti-6Al-4V+TiN composites. Mean values were obtained from the total test duration

4.2.4. Creep properties

In this section the nano-indentation creep behaviour of Ti-6Al-4V+TiN composites was evaluated. The graphs of load-displacement, penetration depth-time, indentation hardness, elastic modulus and indentation creep, were correlated and effects of thermal drift, pileup and sink-in and noise level were taken into consideration.

4.2.4.1 Load-displacement curves

The average load-displacement curves of Ti-6Al-4V+TiN composites are displayed in Figures 4.14 to 4.16. The load-displacement results were obtained from maximum loads of 40 mN, 80 mN, and 100 mN and dwell times of 100s and 200s. All composites displayed smooth curves on loading and unloading curves, with no effects of pop-in effect. It was clear that, the average displacement depth increased on increasing the load from 40 mN to 100 mN and when the dwell time increased from 100 s to 200s. When load increases the penetration depth also increases by virtue of the increase in contact area and high stress (Lin et al., 2009). The increase in dwell time during loading allows enough time for strain-hardening to take place, hence lower penetration depth as the time increases (Dieter and Bacon, 1986).

Increasing the TiN from 0 wt% to 6wt% improved the displacement of Ti-6Al-4V alloy. Ti- 6Al-4V alloy revealed highest displacement depth at all the loads and dwell times as shown in Figure 4.14 to Figure 4.16. Further, when 2 wt% TiN was reinforced the displacement depth began to reduce. However, at 4 wt% TiN, the displacement depth reduced again but tend to increase at 6 wt% TiN.Ti-6Al-4V+6%TiN presented lower displacement depth at 40 mN, 80 mN, and 100 mN. The reduction in penetration depth as the TiN content increased was attributed to the strengthening effect of TiN, which induced the hardness, reduced deformation and improved creep resistance (Shen et al., 2013).

Alternatively, large displacement depth were observed when TiN content increased from 2 wt% to 4wt%. The large discrepancies in the results could be attributed to numerous factors such as, non-uniformity of the material surface which causes nonlinear/fluctuating mechanical properties of the material (Peng et al., 2015). Comparative study conducted by Králík and Němeček (2014), revealed that the heterogeneity of a material can lead to varying penetration depth and hence low average depth due to conflicting mechanical response of each alloy.

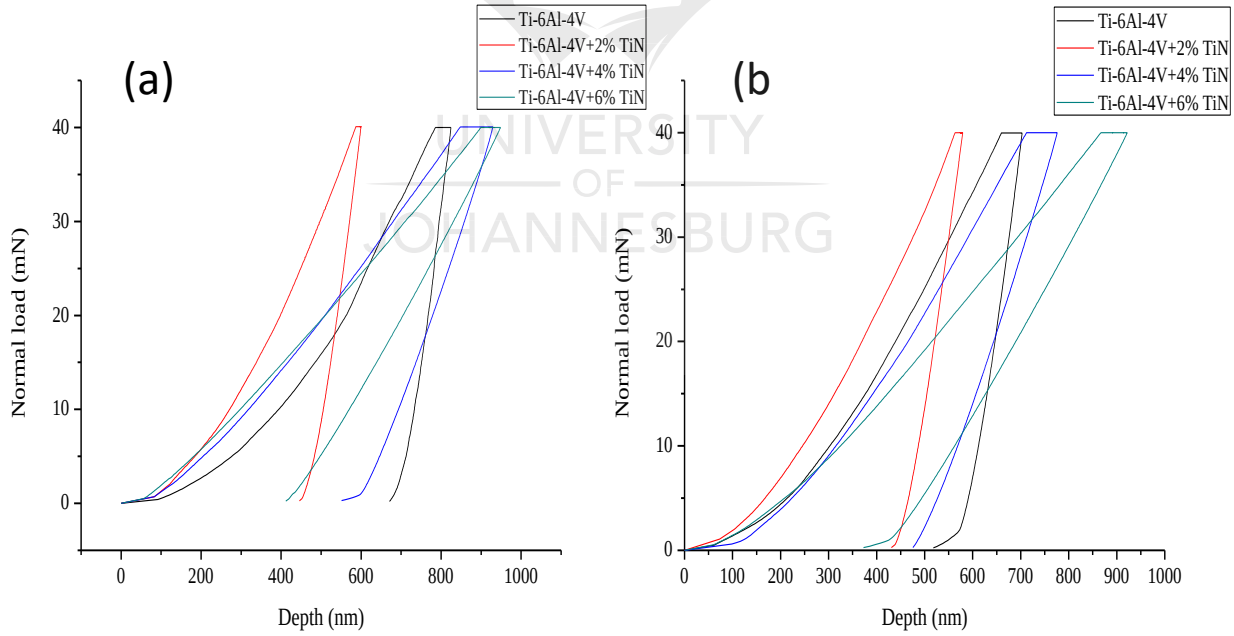

Figure 4. 14.Load displacement curves of Ti-6Al-4V with and without TiN at holding time of (a) 100 s, and (b) 200 s, at a maximum load of 40 mN

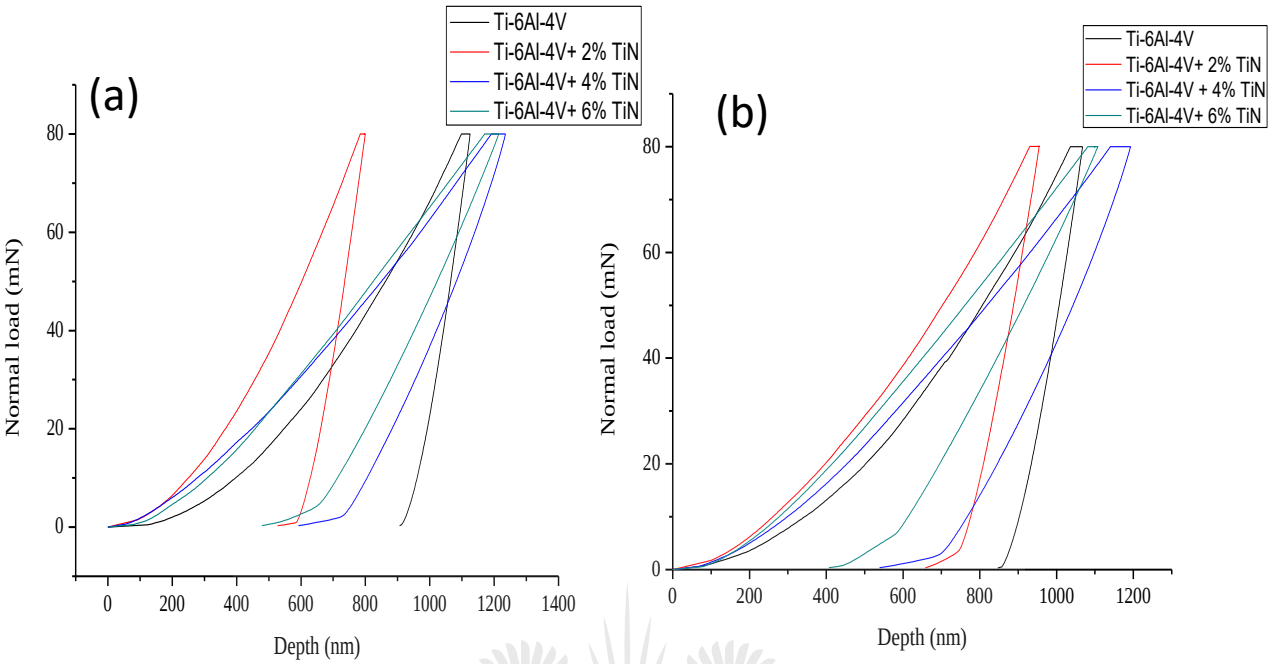

Figure 4. 15. Load displacement curves of Ti-6Al-4V with and without TiN at holding times of (a) 100 s and (b) 200 s, at a maximum load of 80 mN

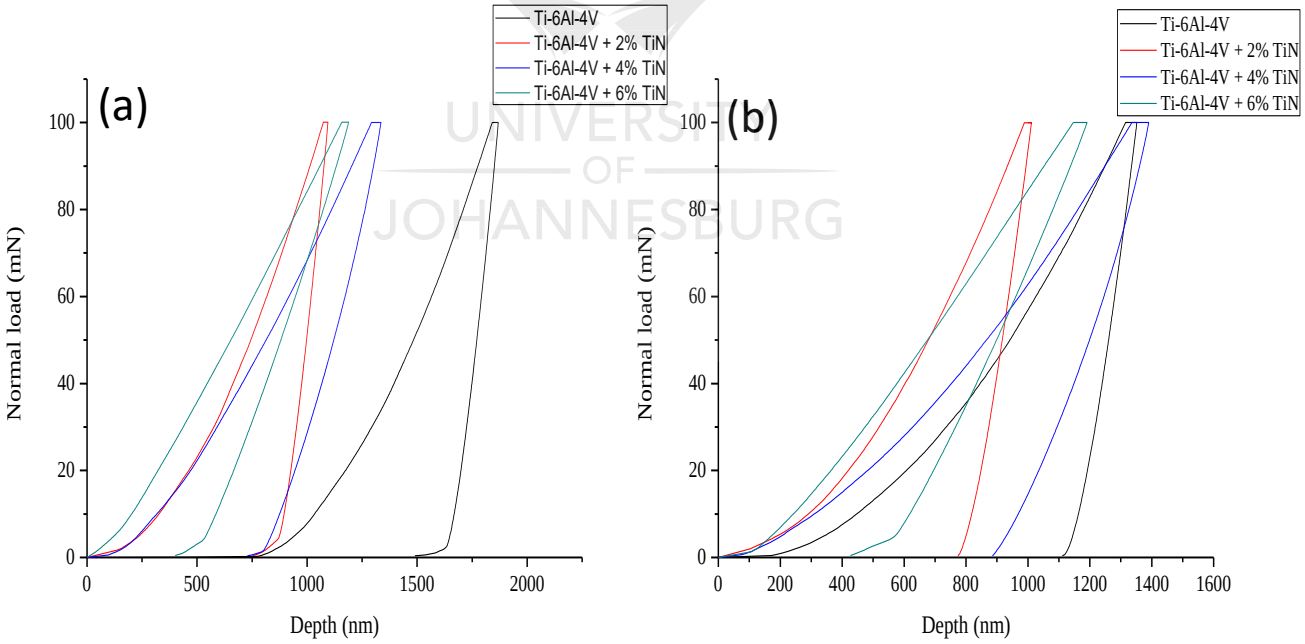

Figure 4. 16. Load displacement curves of Ti-6Al-4V with and without TiN at holding times of (a) 100 s and (b) 200 s, at a maximum load of 100 mN

4.2.4.2 Penetration depth-time curves

The variation of penetration depth with holding time was plotted under test loads of 40, 80 and 100 mN, and dwell time of 100 s and 200 s. The penetration depth-times graphs coincide with the load displacement curves obtained above. The penetration depth increased on increasing the dwell time from 100 s to 200 s. This ascribed to the decrease in stress with time resulting in transformation from elastic strain to plastic strain (Hu et al., 2018).It was observed from Figures 4.17 to 4.19 that the increase in load from 40 to 100 mN resulted in larger creep displacement. Similarly, it was also noticed that penetration depth reduced as TiN content increased. Nanoparticles have the ability to prevent plastic flow, through the dislocation pinning effect, thereby increasing the strength and hardness of a material. Thus, high creep resistance is expected as the volume fraction of nanoparticles increases (Shen et al., 2013). It is worth noting that indentation creep curves do not always show a significant primary stage of creep. The curves depicted two stages (secondary and tertiary stage) of creep curves. Initially, penetration depth increases with time at a decreasing rate until it reaches a steady state where depth and time are directly proportional (Roumina et al., 2004, Yang et al., 2018).

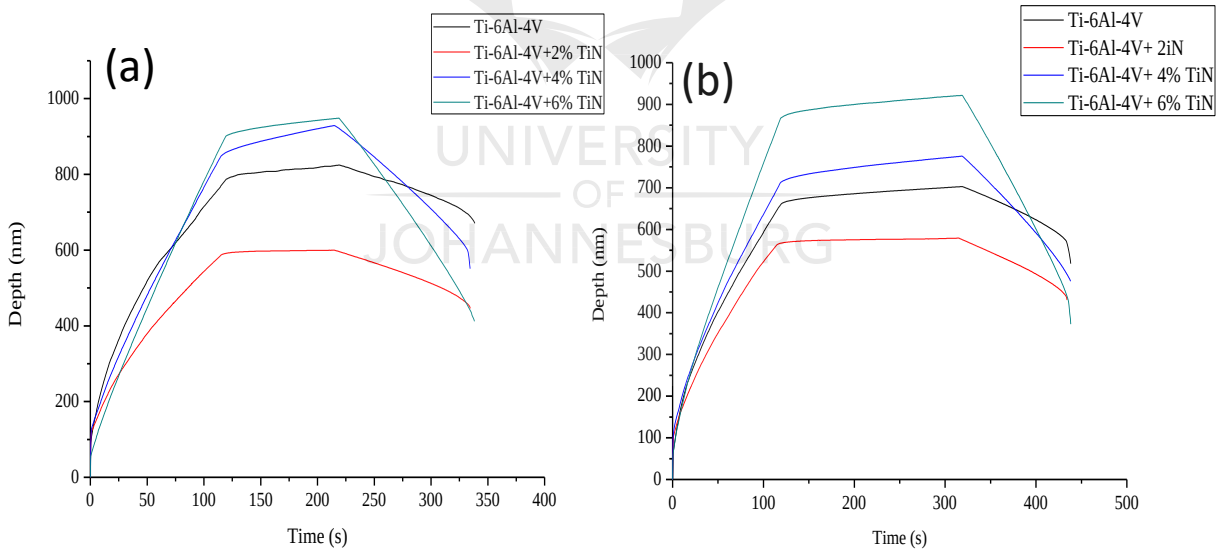

Figure 4. 17. Displacement-holding time curves of Ti-6Al-4V with and without TiN at holding times of (a) 100 s and (b) 200 s, at a maximum load of 40 mN

Ti-6Al-4V+6%TiN yielded small creep displacement at all test durations, as shown in Figure 4.17. Ti-6Al-4V alloy displayed the greatest creep displacement at all dwell times and this trend was maintained at all the loads, as presented in Figure 4.18 and 4.19. It can

be ascertained that increasing the TiN content above 2% could lead to positive impact in mechanical properties at higher loads.

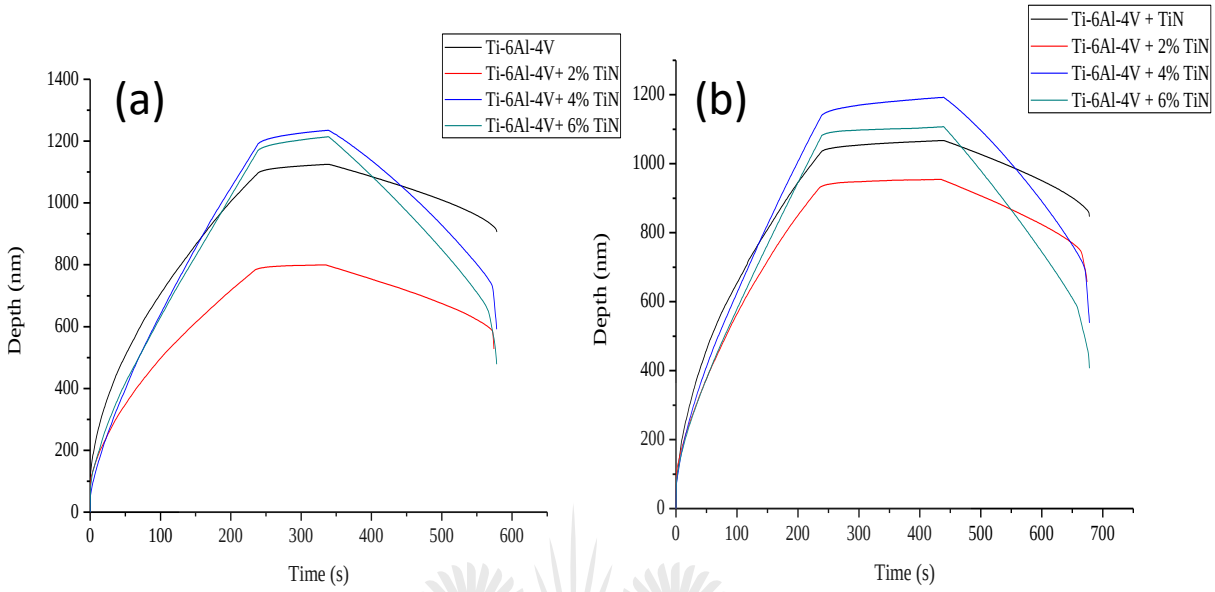

Figure 4. 18. Displacement-holding time curves of Ti-6Al-4V with and without TiN at (a) 100 s, and (b) 200 s, at a maximum load of 80 mN

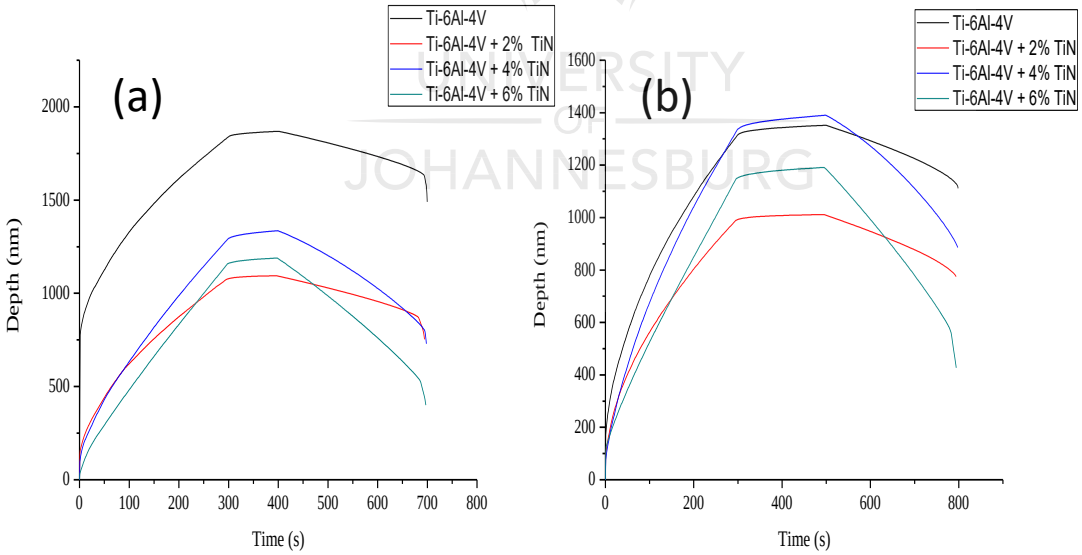

Figure 4. 19. Displacement-holding time curves of Ti-6Al-4V with and without TiN at (a) 100 s, (b) 200 s, at a maximum load of 100 mN

4.2.4.3 Nano indentation hardness against time

The overall indentation hardness results of Ti-6Al-4V alloy increased when TiN nano particles were added. Figure 4.20 shows the bar graph of nanoindetation hardness against dwell time, at

a peak load of 40 mN. Indentation hardness results in this regard were asymmetrical. It was observed that a massive increase in nanoindentation hardness was at Ti6Al-4V+2% TiN, followed by Ti-6Al-4V+6% TiN. Analogously, Maja et al. (2018) found that the hardness of Ti-6Al-4V increased with increase in TiN wt% from Ti-6Al-4V to Ti-6Al-4V+4% TiN. The high hardness in former and the latter was due to the stiff nature of TiN nanoparticles and also homogenous distribution of TiN nanoparticles in Ti-6Al-4V matrix (Shen et al., 2013, Falodun et al., 2018). On the other hand, Ti-6Al-4V alloy presented the lowest nanoindentation hardness at all the test times.

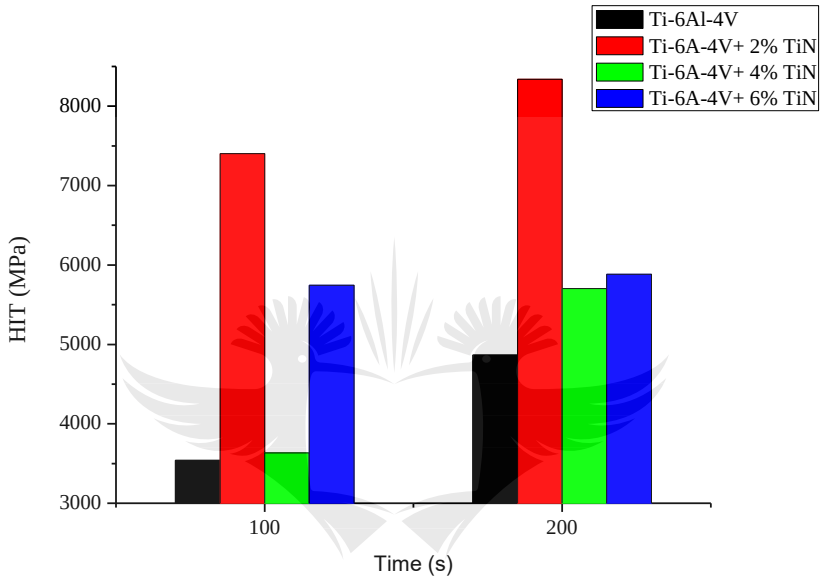

Figure 4. 20. Plots of hardness against holding time at maximum load of 40 mN

Meanwhile, the hardness values at 80 mN are higher than at 40 mN as presented in Figure 4.21. According to Ma et al. (2017) lower indentation loads causes lower penetration depth and high hardness values. Due to limited number of slip systems at lower loads the stress needed to move dislocations or defects increases so as to enhance motion of dislocation. Wang and Lu (2002) reported a decrease in hardness and indentation modulus at the load increased due to indentation size effect. The indentation hardness of crystalline materials displays a strong size effect. The measured indentation hardness of metallic materials typically increases by a factor of two or three as the indentation depth decreases, that is, smaller is harder (Huang et al., 2017).

Moreover, it could be seen that 6% TiN indicated the highest hardness values, which was due to the increase in the volume fraction of TiN nano particles.It should also be noticed that the hardness values of the composites increased with an increase in holding time. The hardness values at 200 s holding time were quite high than at 100 s. It could be inferred that as the

holding time increased enough time is given for dislocation to untangle and move from grain to grain, hence high hardness values.

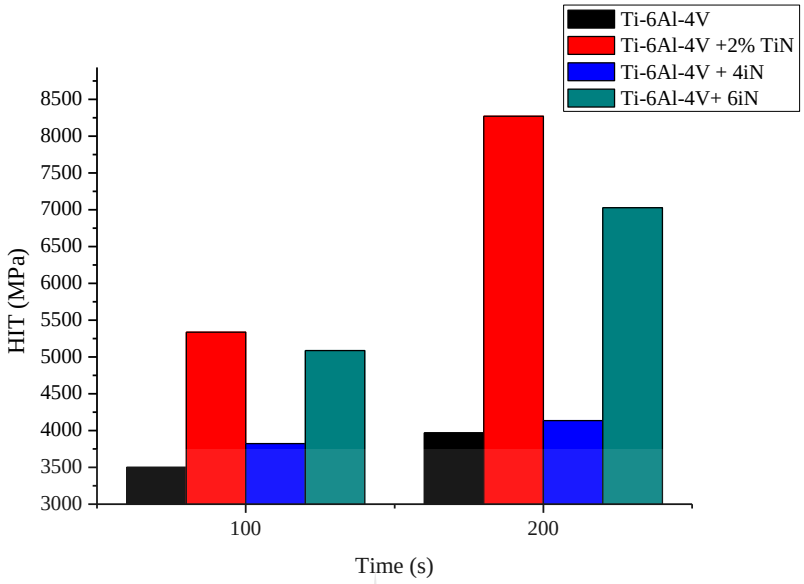

Figure 4. 21. Plots of hardness against holding time at maximum load of 80 mN

Figure 4.22 demonstrates the graph of hardness versus dwell time. An increase in hardness is observed as the dwell time increases. Moreover, a noticeable hardness value of 8200 MPa was noted as the TiN content increases at an indentation load of 100 mN. It is also eminent that at the hardness values increased with dwell time at Ti-6Al-4V, Ti-6Al-4V + 2% TiN and Ti6Al4V+6% TiN. The hardness values at Ti6Al-4V+4% TiN were asymmetrical. Generally, in this situation, 6% TiN has shown high hardness value and Ti-6Al-4V has demonstrated low hardness values.

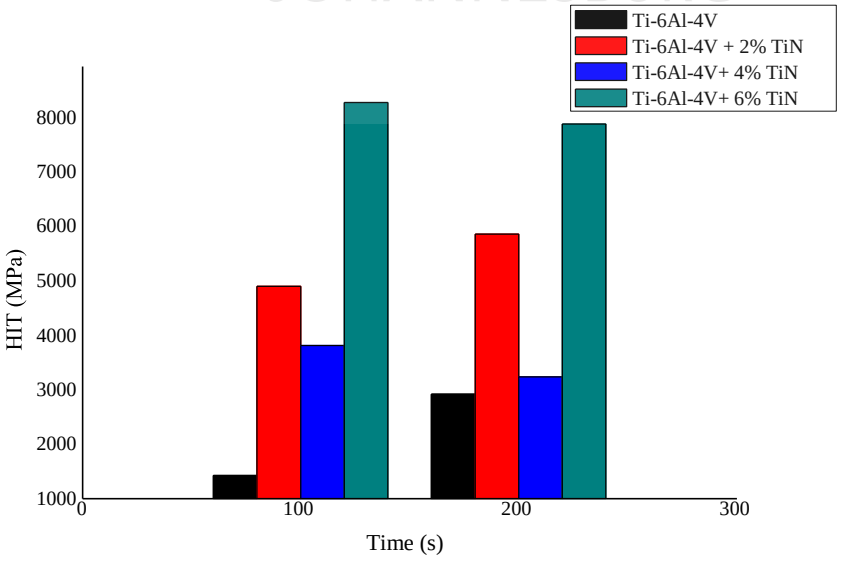

Figure 4. 22. Plots of hardness against holding time at maximum load of 100 mN

It could be deduced that the hardness increased monotonically with an increase in indentation load.Ti6Al-4V without TiN demonstrated lower hardness values, while, 2% and 6%TiN displayed higher hardness values interchangeably. From the results, it is worth noting that there was an increase in hardness from Ti-6Al-4V without TiN to 2%TiN, followed by a reduction in hardness then an increase at 6%TiN.

4.2.4.4 Indentation elastic modulus against TiN ratio Curves

Elastic modulus is a ratio of stress-strain curve in the elastic limit. It is greatly influenced by the matrix and the nanoparticle size addition in a material. Figure 4.23 shows the plots of elastic modulus against TiN addition. At a peak load of 40 mN and dwell times of 100 s and 200 s, Ti6Al-4V+6% TiN presented highest average elastic modulus. It could be inferred that the higher elastic modulus was attributed to the stiff nature of the second phase particles in the matrix. On the other hand, 4% TiN addition resulted in the average lowest elastic modulus. It is worth noting that nonuniformity of the sample surface could lead to non-linear results. Moreover, limited solubility of TiN in Ti-6Al-4V alloy could also cause poor diffusivity of TiN in the alloy matrix and hence average low modulus of elasticity in Ti-6Al-4V+4%TiN (Shen et al., 2013). It could also be observed that all the composites are more responsive to creep at dwell times of 200 s than at 100 s.

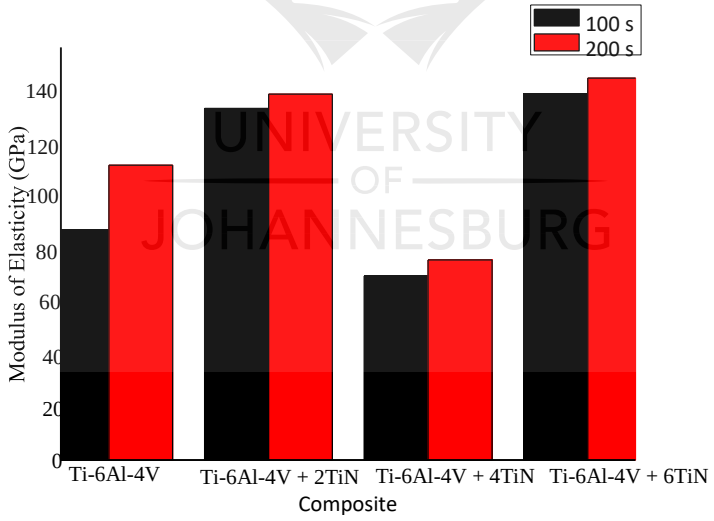

Figure 4. 23. Plots of elastic modulus against TiN composition at holding times of 100 s and 200 s and a load of 40 mN

In Figure 4.24, Ti-6Al-4V+6% TiN exhibited highest average elastic modulus, particularly at 200 s holding time; whereas, Ti-6Al-4V+0% TiN presented slightly lower elastic modulus. Analogous, to what has been observed from load-depth curves, it could be ascertained that 4%TiN yielded lower elastic properties than pure Ti-6Al-4V and 2% TiN. It could be inferred that lack of homogeneity of the surface test piece could cause the former

results. Moreover, it can also be discovered that elastic modulus decreased with increase in load from 40 mN to 80 mN.

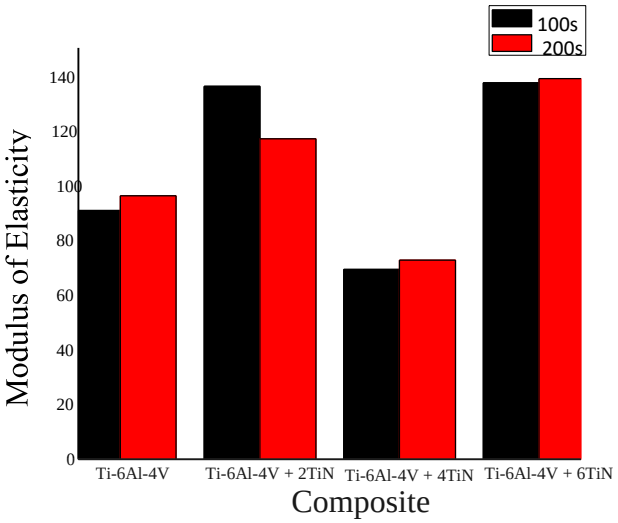

Figure 4. 24. Plots of elastic modulus against TiN composition at holding times of 100 s, 200 s and a load of 80 mN

Figure 4.25 present a graph of elastic modulus versus TiN content at 100 mN .Comparable to 40 mN, 14% reduction in elastic modulus at 100 mN was noted. Average elastic modulus for all the alloys at 40 mN was between 70 GPa and 135 GPa and at 100 mN it was 40 GPa and 119GP. Nonetheless, Ti6A-4V+2% TiN still depicted highest modulus of elasticity at 100 mN at all holding times. Due to greater amount of plastic deformation associated with large loads, the indenter of the material is able to indent into greater depth where the material is more homogeneous resulting in uniform results (Shen et al., 2013). By increasing the peak load, the contact depth becomes deeper and the elastic modulus tends to decrease (Wang and Lu, 2002).

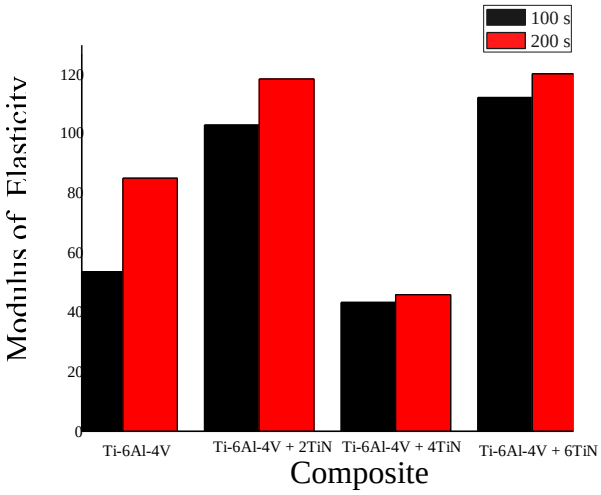

Figure 4. 25. Bar graphs of elastic modulus against TiN composition at holding times of 100 s, 200 s and a load of 100 mN

It can solely can be said that Ti-6Al-4V alloy with 6% TiN presented the highest average modulus of elasticity in all ranges of time 100 and 200 s, while, 4% TiN presented the lowest modulus of elasticity, followed by Ti-6Al-4V alloy. High elastic modulus could be attributed to the strengthening effect of TiN on the interfaces which brings about high stress and strain. (Montecinos et al., 2019, Long et al., 2019) observed an increase in hard as the volume fraction of nanoparticles increased.

4.2.4.5 Stress-strain rate curves and percentage indentation creep results

The representative stress-strain rate curves obtained from Nanoindentation experiments are presented in the Figures 4.26-4.28. The stress-strain rate curves under various maximum indenter loads in the holding stage revealed similar trends. All curves revealed the transient and the steady-state creep stages.

Figure 4.26 shows the stress-strain rate curves for Ti-6Al-4V-TiN composite at a load of 40mN and dwell times of 100s. It was observed that the addition of the TiN content increases the creep resistance of Ti-6Al-4V alloy. The addition of the TiN nanoparticles in Ti-6Al-4V alloy shifts the stress-strain rate curve to higher stress level at nearly the same level of strain rate (Shen et al., 2013). The pristine Ti-6Al-4V alloy showed the highest strain rate (lowest creep resistance) .While Ti-6Al-4V+6TiN showed the lowest strain rate and high stress.

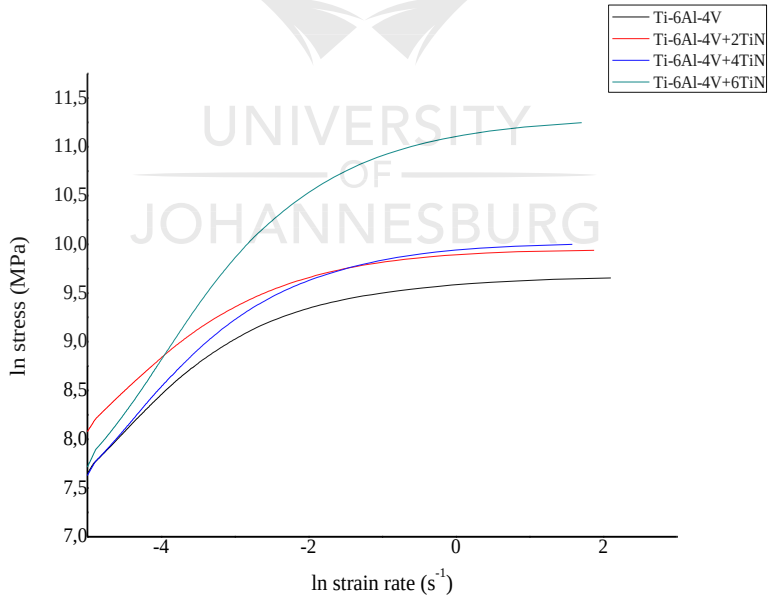

Figure 4. 26. Stress-strain rate curves of Ti-6Al-4V+TiN composite at 40mN and 100s

Stress-strain rate curves of Ti-6Al-4V+TiN composites at a load 80Mn are displayed in Figure 4.27. The composites displayed similar characteristics as in 40mN. Ti-6Al-4V alloy showed the highest creep while Ti-6Al-4V+6TiN revealed the lowest creep properties. The presence of

TiN nano-particles in the Ti-6Al-4V alloy improves the creep properties. Nano-particles hinder the dislocation movement by acting as barriers in the path of dislocation; ultimately dislocations multiply and result in a more strong material (Mouritz, 2012). It is worth-noting that the increased when the load increased. This was attributed to the multiplication of dislocation as the load increases which lead to an increased overall stress of a material (Ma et al., 2017)

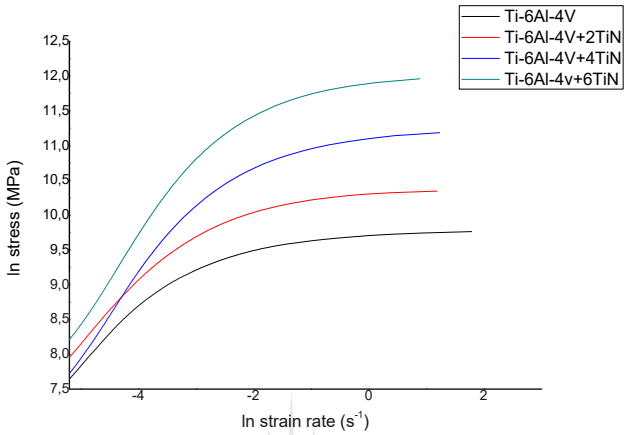

Figure 4. 27. Stress-strain rate curves of Ti-6Al-4V+TiN composite at 80mN and 100s

Figure 4.28 shows the stress-strain rate curve of Ti-6Al-4V+TiN composite at a load of 100mN and dwell time of 100s.The stress strain rate curves presented an increase in stress when the load increased. However, the composites presented an opposite trend when compared to 40mN and 80mN loads. Ti-6Al-4V+2TiN presented high stress at the beginning of load and it decreased when the load increased. The former could be attributed to the creep factors such as the surface finish, inhomogeneity of the alloy at hand. On the same note Ti-6Al-4V presented lowest stress while Ti-6Al-4V+4TiN showed high strain rate (high creep displacement).

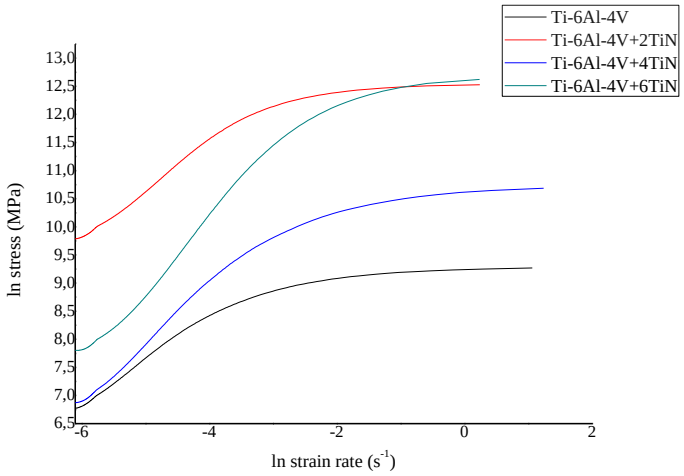

Figure 4. 28. Stress-strain rate curves of Ti-6Al-4V+TiN composite at 100mN and 100s

Figures 4.29 demonstrates a graph of indentation creep as a function of Ti-6Al-4V+ TiN composite, at the applied load of 40 mN and dwell times of 100 s and 200 s. The total indentation creep increased as the dwell time increased from 100s to 200s. Creep is a time dependent plastic deformation of a material, creep is ascribed to the decrease in stress with time resulting in transformation from elastic strain to plastic strain, hence high creep at 200 s (Farokhzadeh and Edrisy, 2015).

On increasing the TiN content to 2 wt% the percentage indentation creep reduced significantly, at 100s and 200s respectively. Conversely, when the TiN content increased to 4 wt% the indentation creep increased but tend to decrease as the TiN content increased to 6 wt%. The aggregate indentation creep of all the composites has increased at 40 mN. The large discrepancies in the results could be attributed to numerous factors such as, non-uniformity of the material surface which causes nonlinear/fluctuating mechanical properties of the material (Peng et al., 2015).

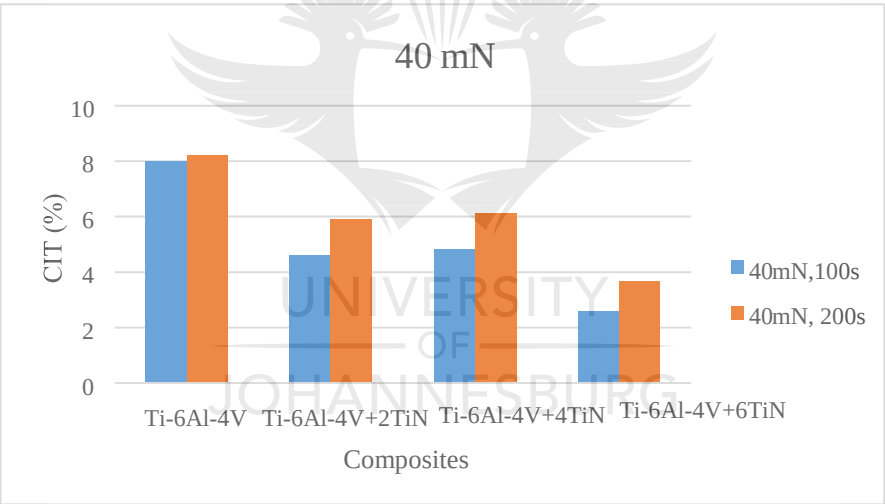

Figure 4. 29. Nanoindentation creep of Ti-6Al-4+ TiN composite at a load of 40 mN

Meanwhile, it was observed in Figure 4.30 that when the load increased from 40 mN to 80 mN the overall indentation creep decreased. Ti-6Al-4V presented high creep deformation at all dwell times. It was then followed by Ti-6Al-4V +4 wt% TiN alloy. Ti-6Al-4V +6%TiN revealed the lowest indentation creep response at all test times. The low creep deformation was due to the presence of hard TiN nanoparticles,which caused resistance to plastic deformation.

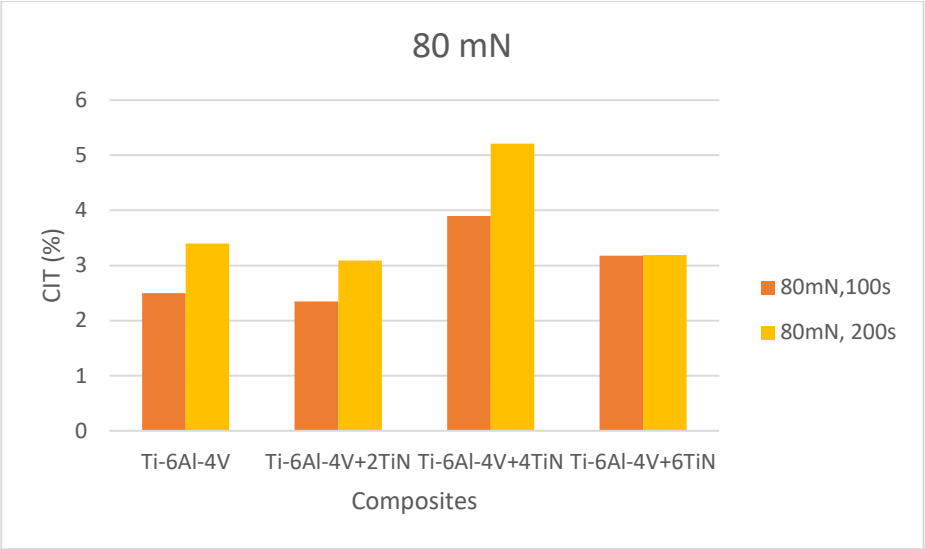

Figure 4. 30. Nanoindentation creep of Ti-6Al-4+ TiN composite at a load of 80 mN

Similar observations were realised at Figure 4.31. Inccreasing TiN content improved the creep deformation of Ti-6Al-4V alloy. Ti-6Al-4V+ 6TiN revealed low creep deformations and Ti6Al-4V presented high creep deformations. However, creep deformations tend to increase when the TiN content was 4 wt%.This could be due to lack of homogenous dispersion of TiN in Ti-6Al-4V matrix.

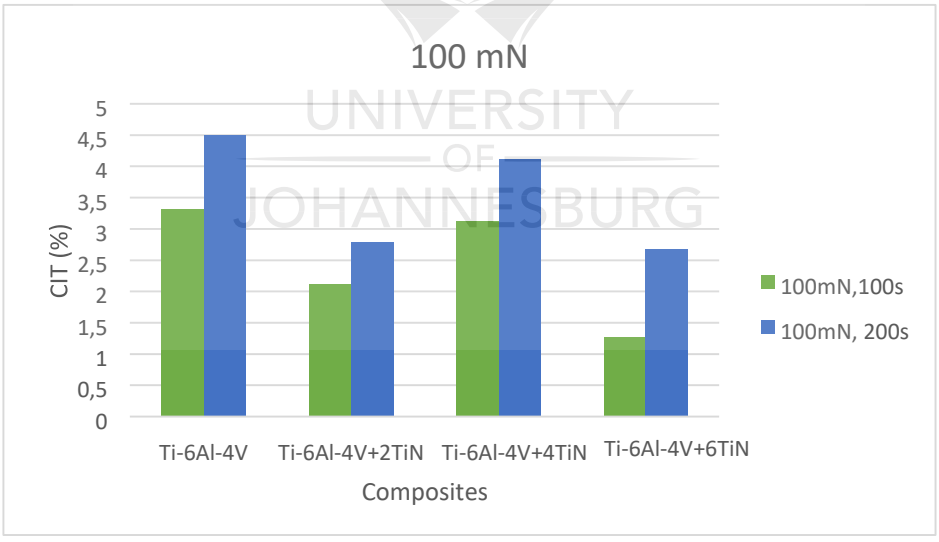

Figure 4. 31. Nanoindetation creep of Ti-6Al-4+ TiN composite at a load of 100mN

CHAPTER FIVE: CONCLUSIONS AND RECOMMENDATIONS

5.1. Conclusions

This study investigated the influence of TiN nanoparticle addition on the erosion-wear, nanoindentation creep and wear properties of spark plasma sintered Ti-6Al-4V alloy. The conclusions are summarised below:

1. The presence of TiN nanoparticles and the spark plasma sintering process in Ti-6Al-4V caused a microstructural change from alpha/beta lamellar to bimodal microstructure.
2. Ti-6Al-4V+6TiN revealed a resistant in erosion wear properties. The presence of TiN nano particles resulted in the strengthening effect of TiN and high hardness properties.
3. Erosion in all alloy composition was dominated by micro-pitting.
4. All the synthesized nanocomposite specimen showed improved wear rate in comparison to Ti-6Al-4V alloy.
5. The hardness and elastic modulus of Ti-6Al-4V+TiN reduced when the load increased from 40 mN to 100 mN.
6. Ti-6Al-4V+2TiN and Ti-6Al-4V +6TiN presented lowest indentation creep properties.
7. Moreover, it is worth noting that load and time had significant effect on the creep behavior of each composite
8. All the composites revealed high wear resistance and creep resistance, when, compared with pure Ti-6Al-4V. However, there was no obvious trend when TiN was added to the Ti-6Al-4V.
9. Finally, bimodal microstructure specimen generated high creep resistance when compared to equiaxed microstructure.

5.2. Recommendations

Developing highly incompressible materials with novel mechanical properties is of highest priority in the high temperature application materials. Moreover, it is significant to understand and ensure that suitable mechanical properties are achieved for engineering use for Ti-6Al-4V alloy when reinforced with TiN as a nanoparticle reinforcement material. It is therefore paramount to understand the contribution of TiN nanoceramic. The following recommendations were suggested so as to deepen the knowledge and understanding and to also increase the market and widen the application range of Ti-6Al-4V alloy.

1. Microstructural evolution plays a very important role when determining material's property. The effect of TiN addition on microstructural evolution revised should be particularly on the matrix and grain boundaries.

2. Atomic force microscope should be used to understand the microstructure of the composite.
3. The mechanical properties of the Ti-6Al-4V+TiN are asymmetrical. In all instances, Ti6Al-4V+4TiN presented lower elastic and plastic properties when compared to Ti-6Al4V+2TiN. Therefore, it can be recommended that the mechanical properties should be examined along the same set of planes for all the samples to avoid fluctuating and erratic results.
4. The original intents of conducting this work was to broaden the application range and enhance the high temperature mechanical properties of Ti-6Al-4V. It is recommended that high temperature nanoindentation studies be conducted on Ti-6Al-4V+TiN composite, to achieve worthwhile properties equivalent to the service condition temperatures

REFERENCES

ABDALLAH, Z., WHITTAKER, M. T. & BACHE, M. R. 2013. High temperature creep behaviour in the γ titanium aluminide Ti–45Al–2Mn–2Nb. *Intermetallics,* 38**,** 55-62.

AHERWAR, A., SINGH, A. K. & PATNAIK, A. 2016. Current and future biocompatibility aspects of biomaterials for hip prosthesis. *AIMS Bioeng,* 3**,** 23-43.

AKBARZADEH, E. 2010. Solid particle erosion of materials for use in gas pipeline control valves.

ALMOTAIRY, S. M., BOOSTANI, A. F., HASSANI, M., WEI, D. & JIANG, Z. Y. 2019. Effect of hot isostatic pressing on the mechanical properties of aluminium metal matrix nanocomposites produced by dual speed ball milling. *Journal of Materials Research and Technology*.

ANTONOV, M., PIRSO, J., VALLIKIVI, A., GOLJANDIN, D. & HUSSAINOVA, I. 2016. The effect of fine erodent retained on the surface during erosion of metals, ceramics, plastic, rubber and hardmetal. *Wear,* 354**,** 53-68.

ASHBY, M. F. & JONES, D. R. H. 2012. *Engineering materials 1: an introduction to properties, applications and design*. United Kingdom:Cambridge

AZARNIYA, A., COLERA, X. G., MIRZAALI, M. J., SOVIZI, S., BARTOLOMEU, F., WITS, W. W., YAP, C. Y., AHN, J., MIRANDA, G. & SILVA, F. S. 2019. Additive manufacturing of Ti–6Al–4V parts through laser metal deposition (LMD): Process, microstructure, and mechanical properties. *Journal of Alloys and Compounds*.8, 163-191

BADEA, L., SURAND, M., RUAU, J. & VIGUIER, B. 2013. Creep behavior of Ti-6Al-4V from 450° C to 600° C. *University Polytechnica of Bucharest Scientific Bulletin, Series B,* 76**,** 185-196.

BAHAIDEEN, F. B., SALEEM, A. M., HUSSAIN, K., RIPIN, Z., AHMAD, Z., SAMAD, Z. & BADARULZAMAN, N. 2009. Fatigue behaviour of aluminum alloy at elevated temperature. *Modern applied science,* 3**,** 52-61.

BAYODE, B. L. 2016. Spark Plasma Sintering of Titanium-Zirconium-Tantalum High Temperature Shape Memory Alloy.

BHUSHAN, B. & GUPTA, B. K. 1991. Handbook of tribology: materials, coatings, and surface treatments.

BRIGUENTE, L., COUTO, A. A., GUIMARÃES, N. M., REIS, D. A., DE MOURA NETO, C. & BARBOZA, M. Determination of creep parameters of Ti-6Al-4V with

bimodal and equiaxed microstructure. Defect and Diffusion Forum, 2012. Trans Tech Publ, 520524.

CARDINAL, S., MALCHERE, A., GARNIER, V. & FANTOZZI, G. 2009. Microstructure and mechanical properties of TiC–TiN based cermets for tools application. *International Journal of Refractory Metals and Hard Materials,* 27**,** 521-527.

CARRION, P. E., SHAMSAEI, N., DANIEWICZ, S. R. & MOSER, R. D. 2017. Fatigue behavior of Ti-6Al-4V ELI including mean stress effects. *International Journal of Fatigue,* 99**,** 87-100.

CHEN, C. 2009. 2-D finite element modeling for nanoindentation and fracture stress analysis.

CHEN, X., XIANG, Y. & VLASSAK, J. J. 2006. Novel technique for measuring the mechanical properties of porous materials by nanoindentation. *Journal of Materials Research,* 21**,** 715-724.

CHMIELA, B., KOŚCIELNIAK, B. & ROSKOSZ, S. 2016. Characterizing the Effects of Hot Isostatic Pressing on IN713C Superalloy Blade Microstructure by Electron Backscatter Diffraction. *Acta Physica Polonica A,* 130**,** 1097-1099.

DAI, J., ZHU, J., CHEN, C. & WENG, F. 2016. High temperature oxidation behavior and research status of modifications on improving high temperature oxidation resistance of titanium alloys and titanium aluminides: A review. *Journal of Alloys and Compounds,* 685**,** 784-798.

DIETER, G. E. & BACON, D. J. 1986. *Mechanical metallurgy,* McGraw-hill New York.

DONACHIE JR, M. J. 2000. Introduction to selection of titanium alloys. *Titanium-A Technical Guide***,** 5-10.

EGART, M., JANKOVIĆ, B. & SRČIČ, S. 2016. Application of instrumented nanoindentation in preformulation studies of pharmaceutical active ingredients and excipients. *Acta Pharmaceutica,* 66**,** 303-330.

ELIAS, C. N., MEYERS, M. A., VALIEV, R. Z. & MONTEIRO, S. N. 2013. Ultrafine grained titanium for biomedical applications: An overview of performance. *Journal of Materials Research and Technology,* 2**,** 340-350.

ESSA, K., KHAN, R., HASSANIN, H., ATTALLAH, M. M. & REED, R. 2016. An iterative approach of hot isostatic pressing tooling design for net-shape IN718 superalloy parts. *The International Journal of Advanced Manufacturing Technology,* 83**,** 1835-1845.

ETTMAYER, P., KOLASKA, H., LENGAUER, W. & DREYER, K. 1995. Ti (C, N) cermets—metallurgy and properties. *International Journal of Refractory Metals and Hard Materials,* 13**,** 343-351.

FALODUN, O. E., OBADELE, B. A., OKE, S. R., MAJA, M. E. & OLUBAMBI, P. A. 2018. Effect of sintering parameters on densification and microstructural evolution of nanosized titanium nitride reinforced titanium alloys. *Journal of Alloys and Compounds,* 736**,** 202-210.

FAROKHZADEH, K. & EDRISY, A. 2015. Fatigue improvement in low temperature plasma nitrided Ti–6Al–4V alloy. *Materials Science and Engineering: A,* 620**,** 435-444.

FISCHER-CRIPPS, A. C. 2011. Nanoindentation testing. *Nanoindentation.* Springer.

GHIBAN, B., BRAN, D.-T. & ELEFTERIE, C. F. (2018,February). Requirements of titanium alloys for aeronautical industry. Retrieved from: 10.1063/1.5024165.Accessed on: 20 Novemver 2019

GOLLAPUDI, S., SATYANARAYANA, D. V. V., PHANIRAJ, C. & NANDY, T. K. 2012. Transient creep in titanium alloys: Effect of stress, temperature and trace element concentration. *Materials Science and Engineering: A,* 556**,** 510-518.

GOULDSTONE, A., KOH, H.-J., ZENG, K.-Y., GIANNAKOPOULOS, A. & SURESH, S. 2000. Discrete and continuous deformation during nanoindentation of thin films. *Acta Materialia,* 48**,** 2277-2295.

GUO, R., XU, L., WU, J., YANG, R. & ZONG, B. Y. 2015. Microstructural evolution and mechanical properties of powder metallurgy Ti–6Al–4V alloy based on heat response. *Materials Science and Engineering: A,* 639**,** 327-334.

GUPTA, P., KUMAR, D., PARKASH, O., JHA, A. K. & SADASIVUNI, K. K. 2018. Dependence of wear behavior on sintering mechanism for Iron-Alumina Metal Matrix Nanocomposites. *Materials Chemistry and Physics,* 220**,** 441-448.

GURRAPPA, I. 2005. An oxidation model for predicting the life of titanium alloy components in gas turbine engines. *Journal of Alloys and Compounds,* 389**,** 190-197.

HAN, L., SPANGSDORF, S. H., NONG, N., HUNG, L., ZHANG, Y., PHAM, H. N., CHEN, Y., ROCH, A., STEPIEN, L. & PRYDS, N. 2016. Effects of spark plasma sintering conditions on the anisotropic thermoelectric properties of bismuth antimony telluride. *RSC Advances,* 6**,** 59565-59573.

HU, J., ZHANG, W., PENG, G., ZHANG, T. & ZHANG, Y. 2018. Nanoindentation deformation of refine-grained AZ31 magnesium alloy: indentation size effect, pop-in effect and creep behavior. *Materials Science and Engineering: A,* 725**,** 522-529.

HUANG, S., MA, Y., QIU, J., WANG, H., LEI, J., ZONG, B. Y. & YANG, R. 2017. Enhanced ambient temperature creep resistance of α/β-Ti alloys induced by minor Fe. *Materials Science and Engineering: A,* 705**,** 169-175.

JIANG, J., XU, X. & STRINGER, J. 2018. Support Structures for Additive Manufacturing: A Review. *Journal of Manufacturing and Materials Processing,* 2**,** 64.

KAMAL, M. & RAHMAN, M. 2018. Advances in fatigue life modeling: A review. *Renewable and Sustainable Energy Reviews,* 82**,** 940-949.

KASSNER, M. E. 2015. *Fundamentals of creep in metals and alloys*, Butterworth-Heinemann.

KGOETE, F., FAYOMI, O. & ADEBIYI, I. 2018. Influence of Si3N4 on Ti-6Al-4V via spark plasma sintering: Microstructure, corrosion and thermal stability. *Journal of Alloys and Compounds,* 763**,** 322-328.

KOSA, E. & GÖKSENLI, A. 2017. Influence of material hardness and particle velocity on erosive wear rate. *Journal of Mechanical Engineering,* 47**,** 9-15.

KOVAŘÍKOVÁ, I., SZEWCZYKOVÁ, B., BLAŠKOVIŠ, P., HODÚLOVÁ, E. & LECHOVIČ, E. 2009. Study and characteristic of abrasive wear mechanisms. *Materials Science and Technology [online]*.1**,** 1335-9053.

KRÁLÍK, V. & NĚMEČEK, J. 2014. Comparison of nanoindentation techniques for local mechanical quantification of aluminium alloy. *Materials Science and Engineering: A,* 618**,** 118-128.

LIN, Y., WENG, Y., PEN, D. & LI, H. 2009. Deformation model of brittle and ductile materials under nano-indentation. *Materials & Design,* 30**,** 1643-1649.

LIU, P., ZONG, Y., SHAN, D. & GUO, B. 2015. Relationship between constant-load creep, decreasing-load creep and stress relaxation of titanium alloy. *Materials Science and Engineering: A,* 638**,** 106-113.

LIU, Y., HUANG, C., BEI, H., HE, X. & HU, W. 2012. Room temperature nanoindentation creep of nanocrystalline Cu and Cu alloys. *Materials Letters,* 70**,** 26-29.

LONG, X., HU, B., FENG, Y., CHANG, C. & LI, M. 2019. Correlation of microstructure and constitutive behaviour of sintered silver particles via nanoindentation. *International Journal of Mechanical Sciences,* 161**,** 20-26.

LUCCA, D. A., HERRMANN, K. & KLOPFSTEIN, M. J. 2010. Nanoindentation: Measuring methods and applications. *CIRP Annals,* 59**,** 803-819.

MA, X., LI, F., ZHAO, C., ZHU, G., LI, W., SUN, Z. & YUAN, Z. 2017. Indenter load effects on creep deformation behavior for Ti-10V-2Fe-3Al alloy at room temperature. *Journal of Alloys and Compounds,* 709**,** 322-328.

MAHESH, L., SUDHEER REDDY, J. & MUKUNDA, P. 2017. Development and characterization of titanium nitride reinforced aluminium MMC's through powder metallurgy technique. *Mechanics and Mechanical Engineering,* 21**,** 29-36.

MAJA, M. E., FALODUN, O. E., OBADELE, B. A., OKE, S. R. & OLUBAMBI, P. A. 2018. Nanoindentation studies on TiN nanoceramic reinforced Ti–6Al–4V matrix composite. *Ceramics International,* 44**,** 4419-4425.

MARWALA, T. & HURWITZ, E. 2017. Introduction to man and machines. *Artificial Intelligence and Economic Theory: Skynet in the Market.*South Africa

MAZERAN, P.-E., BEYAOUI, M., BIGERELLE, M. & GUIGON, M. 2012. Determination of mechanical properties by nanoindentation in the case of viscous materials. *International Journal of Materials Research,* 103**,** 715-722.

MONTECINOS, S., TOGNANA, S. & SALGUEIRO, W. 2019. Influence of pile-up on nanoindentation measurements in Cu–2wt.% Be samples with precipitates. *Transactions of Nonferrous Metals Society of China,* 29**,** 2340-2350.

MOORHOUSE, B. 2013. Controlling the interstitial element concentration in Ti-6Al-4V using calciothermic reduction.https://doi.org/10.25560/12682.Retrieved on:03 May 2017 .

MOURITZ, A. P. 2012. *Introduction to aerospace materials*. 80 High Street, Sawston, Cambridge, CB22 3HJ, UK. 2012. 621pp.

MPHAHLELE, M. R. 2018. *Mechanical and tribological properties of nanoceramics dispersion strengthened 2205 duplex stainless steel.* University of Johannesburg. Retrieved:https://ujcontent.uj.ac.za/vital/access/manager/Index?site_name=Research%20Output. Accessed on:21 November 2018

MUHAMMAD, M., MASOOMI, M., TORRIES, B., SHAMSAEI, N. & HAGHSHENAS, M. 2018. Depth-sensing time-dependent response of additively manufactured Ti-6Al-4V alloy. *Additive Manufacturing,* 24**,** 37-46.

NAVEED, M., RENTERIA, A. F., NEBEL, D. & WEIß, S. 2015. Study of high velocity solid particle erosion behaviour of Ti2AlC MAX phase coatings. *Wear,* 342-343**,** 391-397.

OBADELE, B. A. 2014.Tribocorrosion mechanisms in laser deposited titanium-based smart composite coatings.Retrieved from:http://encore.tut.ac.za/iii/cp.Accessed on: May 2017

PENG, G., MA, Y., FENG, Y., HUAN, Y., QIN, C. & ZHANG, T. 2015. Nanoindentation creep of nonlinear viscoelastic polypropylene. *Polymer Testing,* 43**,** 38-43.

POLMEAR, I., STJOHN, D., NIE, J.-F. & QIAN, M. 2017. *Light alloys: metallurgy of the light metals*, Butterworth-Heinemann.

REED-HILL, R. E., ABBASCHIAN, R. & ABBASCHIAN, R. 1973. *Physical metallurgy principles.* United States of America: University of Florida

ROUMINA, R., RAEISINIA, B. & MAHMUDI, R. 2004. Room temperature indentation creep of cast Pb–Sb alloys. *Scripta materialia,* 51**,** 497-502.

RUSSIAS, J., CARDINAL, S., AGUNI, Y., FANTOZZI, G., BIENVENU, K. & FONTAINE, J. 2005. Influence of titanium nitride addition on the microstructure and mechanical properties of TiC-based cermets. *International Journal of Refractory Metals and Hard Materials,* 23**,** 358-362.

SAHEB, N., IQBAL, Z., KHALIL, A., HAKEEM, A. S., AL AQEELI, N., LAOUI, T., ALQUTUB, A. & KIRCHNER, R. 2012. Spark plasma sintering of metals and metal matrix nanocomposites: a review. *Journal of Nanomaterials,* 2012**,** 18-31.

SATO, E., YAMADA, T., TANAKA, H. & JIMBO, I. 2006. Categorization of ambienttemperature creep behavior of metals and alloys on their crystallographic structures. *Materials transactions,* 47**,** 1121-1126.

SAXENA, A., SINGH, N., KUMAR, D. & GUPTA, P. 2017. Effect of Ceramic Reinforcement on the Properties of Metal Matrix Nanocomposites. *Materials Today: Proceedings,* 4**,** 5561-5570.

SHARMA, S. K., SELOKAR, A. W., KUMAR, B. V. M. & VENKATESWARAN, T. 2017. High temperature erosion behavior of spark plasma sintered ZrB2-SiC composites. *Ceramics International,* 43**,** 8982-8988.

SHEN, L., TAN, Z. Y. & CHEN, Z. 2013. Nanoindentation study on the creep resistance of SnBi solder alloy with reactive nano-metallic fillers. *Materials Science and Engineering: A,* 561**,** 232-238.

SHI, Z., YIN, D., ZHANG, D. & LIU, X. 2017. Characterisation of Ti (C, N)-based cermets with various nitrogen contents studied by EBSD/SEM and TEM. *Journal of Alloys and Compounds,* 695**,** 2857-2864.

STACHOWIAK, G., PODSIADLO, P. & STACHOWIAK, G. 2006. Shape and texture features in the automated classification of adhesive and abrasive wear particles. *Tribology*

Letters, 24**,** 15-26.

SUN, Y., CHEN, Y., WANG, X. & TANG, X. Deep learning face representation by joint identification-verification. *Advances in neural information processing systems,* 2014. 1988-1996.

SUNDARARAJAN, G. & ROY, M. 1997. Solid particle erosion behaviour of metallic materials at room and elevated temperatures. *Tribology International,* 30**,** 339-359.

TAKAHASHI, M. 2003. Development of high strength steels for automobiles. *Shinnittetsu Giho*, 2-6.

TAM, C.-H., LEE, S.-C. & CHANG, S.-H. 2009. The Influence of Canning HIP Treatment on the Microstructure Characters of Cr_{35}-Si_{65} and Cr_{50}-Si_{50} Targets. *Materials transactions,* 50**,** 885-890.

TAMMAS-WILLIAMS, S., WITHERS, P. J., TODD, I. & PRANGNELL, P. B. 2016. The effectiveness of hot isostatic pressing for closing porosity in titanium parts manufactured by selective electron beam melting. *Metallurgical and Materials Transactions A,* 47**,** 1939-1946.

TAO, J., FENG, Y. & TANG, K. 2014. Fatigue crack detection for a structural hotspot. *Journal of Measurements in Engineering,* 2**,** 49-56.

VEIGA, C., DAVIM, J. P. & LOUREIRO, A. J. R. 2012. Properties and applications of titanium alloys: a brief review. *Materials Science and Engineering,* 32**,** 133-148.

WANG, H.-B., WANG, S.-S., GAO, P.-Y., JIANG, T., LU, X.-G. & LI, C.-H. 2016. Microstructure and mechanical properties of a novel near-α titanium alloy Ti6. 0Al4. 5Cr1. 5Mn. *Materials Science and Engineering: A,* 672**,** 170-174.

WANG, W. & LU, K. 2002. Nanoindentation measurement of hardness and modulus anisotropy in Ni 3 Al single crystals. *Journal of materials research,* 17**,** 2314-2320.

WATKINS, G. 2015. Development of a high temperature titanium alloy for gas turbine applications. Retrieved from: https://doi.org/10.1080/09603409.2016.1184423.Accessed on: 23 November 2019

WHEELER, J. M. 2009. *Nanoindentation under dynamic conditions.* University of Cambridge.Retrieved from: https://core.ac.uk/download/pdf/1316450.pdf.Accessed on:23 November 2019

WOODING, V. K. & LAUBSCHER, R. F. 2014. Variable Length Scale Surface Finish Assessment of Machined Grade 4 Titanium Alloy. *Procedia CIRP,* 13**,** 90-96.

WU, B., MYANT, C. & WEIDER, S. Z. 2017. The value of additive manufacturing: future opportunities.Retrieved from: https://manufacturing.report/view-resource.aspx?id=3438. Accessed on:23 November 2019

YAMADA, M. 1996. An overview on the development of titanium alloys for non-aerospace application in Japan. *Materials Science and Engineering: A,* 213**,** 8-15.

YANG, X.-S., ZHAI, H.-R., RUAN, H.-H., SHI, S.-Q. & ZHANG, T.-Y. 2018. Multitemperature indentation creep tests on nanotwinned copper. *International Journal of Plasticity,* 104**,** 68-79.

YU, S., ZENG, Q., OGANOV, A. R., FRAPPER, G. & ZHANG, L. 2015. Phase stability, chemical bonding and mechanical properties of titanium nitrides: a first-principles study. *Physical Chemistry Chemical Physics,* 17**,** 11763-11769.

YU, W. H., SING, S. L., CHUA, C. K., KUO, C. N. & TIAN, X. L. 2019. Particle-reinforced metal matrix nanocomposites fabricated by selective laser melting: A state of the art review. *Progress in Materials Science,* 104**,** 330-379.

ZGALAT-LOZYNSKYY, O., HERRMANN, M., RAGULYA, A., ANDRZEJCZUK, M. & POLOTAI, A. 2012. Structure and mechanical properties of spark plasma sintered TiNbased nanocomposites. *Archives of Metallurgy and Materials,* 57**,** 853-858.

ZHANG, J., LANSDALE, P. A. & LYNN, D. M. 2014. Liu et al. *Polymer,* 90**,** 90.

ZHANG, W.-D., LIU, Y., WU, H., LAN, X.-D., QIU, J., HU, T. & TANG, H.-P. 2016. Room temperature creep behavior of Ti–Nb–Ta–Zr–O alloy. *Materials Characterization,* 118**,** 29-36.

ZHAO, J., HUANG, P., XU, K., WANG, F. & LU, T. 2018. Indentation size and loading strain rate dependent creep deformation of nanocrystalline Mo. *Thin Solid Films,* 653**,** 365370.

ZHOU, S., YANG, C.-H., LIN, S.-K., ALHAZAA, A. N., MOKHTARI, O., LIU, X. & NISHIKAWA, H. 2019. Effects of Ti addition on the microstructure, mechanical properties and electrical resistivity of eutectic Sn58Bi alloy. *Materials Science and Engineering: A,* 744**,** 560-569.

ZHOU, S., ZHAO, W. & XIONG, W. 2009. Microstructure and properties of the cermets based on Ti (C, N). *International Journal of Refractory Metals and Hard Materials,* 27**,** 26-32.